EUROPEAN ORGANIZATION FOR NUCLEAR RESEARCH

Leading Particle Production in Light Flavour Jets

The OPAL Collaboration

Abstract

The energy distribution and type of the particle with the highest momentum in quark jets are determined for each of the five quark flavours making only minimal model assumptions. The analysis is based on a large statistics sample of hadronic Z^0 decays collected with the OPAL detector at the LEP e^+e^- collider. These results provide a basis for future studies of light flavour production at other centre-of-mass energies. We use our results to study the hadronisation mechanism in light flavour jets and compare the data to the QCD models JETSET and HERWIG. Within the JETSET model we also directly determine the suppression of strange quarks to be

$$\gamma_s = 0.422 \pm 0.049(\text{stat.}) \pm 0.059(\text{syst.})$$

by comparing the production of charged and neutral kaons in strange and non-strange light quark events. Finally we study the features of baryon production.

(Submitted to Eur. Phys. Jour. C)

The OPAL Collaboration

G. Abbiendi[2], K. Ackerstaff[8], P.F. Akesson[3], G. Alexander[23], J. Allison[16], K.J. Anderson[9],
S. Arcelli[17], S. Asai[24], S.F. Ashby[1], D. Axen[29], G. Azuelos[18,a], I. Bailey[28], A.H. Ball[8],
E. Barberio[8], R.J. Barlow[16], J.R. Batley[5], S. Baumann[3], T. Behnke[27], K.W. Bell[20],
G. Bella[23], A. Bellerive[9], S. Bentvelsen[8], S. Bethke[14,i], S. Betts[15], O. Biebel[14,i],
A. Biguzzi[5], I.J. Bloodworth[1], P. Bock[11], J. Böhme[14,h], O. Boeriu[10], D. Bonacorsi[2],
M. Boutemeur[33], S. Braibant[8], P. Bright-Thomas[1], L. Brigliadori[2], R.M. Brown[20],
H.J. Burckhart[8], P. Capiluppi[2], R.K. Carnegie[6], A.A. Carter[13], J.R. Carter[5],
C.Y. Chang[17], D.G. Charlton[1,b], D. Chrisman[4], C. Ciocca[2], P.E.L. Clarke[15], E. Clay[15],
I. Cohen[23], J.E. Conboy[15], O.C. Cooke[8], J. Couchman[15], C. Couyoumtzelis[13], R.L. Coxe[9],
M. Cuffiani[2], S. Dado[22], G.M. Dallavalle[2], S. Dallison[16], R. Davis[30], A. de Roeck[8],
P. Dervan[15], K. Desch[27], B. Dienes[32,h], M.S. Dixit[7], M. Donkers[6], J. Dubbert[33],
E. Duchovni[26], G. Duckeck[33], I.P. Duerdoth[16], P.G. Estabrooks[6], E. Etzion[23], F. Fabbri[2],
A. Fanfani[2], M. Fanti[2], A.A. Faust[30], L. Feld[10], P. Ferrari[12], F. Fiedler[27], M. Fierro[2],
I. Fleck[10], A. Frey[8], A. Fürtjes[8], D.I. Futyan[16], P. Gagnon[12], J.W. Gary[4], G. Gaycken[27],
C. Geich-Gimbel[3], G. Giacomelli[2], P. Giacomelli[2], D.M. Gingrich[30,a], D. Glenzinski[9],
J. Goldberg[22], W. Gorn[4], C. Grandi[2], K. Graham[28], E. Gross[26], J. Grunhaus[23],
M. Gruwé[27], C. Hajdu[31] G.G. Hanson[12], M. Hansroul[8], M. Hapke[13], K. Harder[27],
A. Harel[22], C.K. Hargrove[7], M. Harin-Dirac[4], M. Hauschild[8], C.M. Hawkes[1],
R. Hawkings[27], R.J. Hemingway[6], G. Herten[10], R.D. Heuer[27], M.D. Hildreth[8], J.C. Hill[5],
P.R. Hobson[25], A. Hocker[9], K. Hoffman[8], R.J. Homer[1], A.K. Honma[8], D. Horváth[31,c],
K.R. Hossain[30], R. Howard[29], P. Hüntemeyer[27], P. Igo-Kemenes[11], D.C. Imrie[25], K. Ishii[24],
F.R. Jacob[20], A. Jawahery[17], H. Jeremie[18], M. Jimack[1], C.R. Jones[5], P. Jovanovic[1],
T.R. Junk[6], N. Kanaya[24], J. Kanzaki[24], G. Karapetian[18], D. Karlen[6], V. Kartvelishvili[16],
K. Kawagoe[24], T. Kawamoto[24], P.I. Kayal[30], R.K. Keeler[28], R.G. Kellogg[17],
B.W. Kennedy[20], D.H. Kim[19], A. Klier[26], T. Kobayashi[24], M. Kobel[3], T.P. Kokott[3],
M. Kolrep[10], S. Komamiya[24], R.V. Kowalewski[28], T. Kress[4], P. Krieger[6], J. von Krogh[11],
T. Kuhl[3], M. Kupper[26], P. Kyberd[13], G.D. Lafferty[16], H. Landsman[22], D. Lanske[14],
J. Lauber[15], I. Lawson[28], J.G. Layter[4], D. Lellouch[26], J. Letts[12], L. Levinson[26],
R. Liebisch[11], J. Lillich[10], B. List[8], C. Littlewood[5], A.W. Lloyd[1], S.L. Lloyd[13],
F.K. Loebinger[16], G.D. Long[28], M.J. Losty[7], J. Lu[29], J. Ludwig[10], A. Macchiolo[18],
A. Macpherson[30], W. Mader[3], M. Mannelli[8], S. Marcellini[2], T.E. Marchant[16],
A.J. Martin[13], J.P. Martin[18], G. Martinez[17], T. Mashimo[24], P. Mättig[26],
W.J. McDonald[30], J. McKenna[29], E.A. Mckigney[15], T.J. McMahon[1], R.A. McPherson[28],
F. Meijers[8], P. Mendez-Lorenzo[33], F.S. Merritt[9], H. Mes[7], I. Meyer[5], A. Michelini[2],
S. Mihara[24], G. Mikenberg[26], D.J. Miller[15], W. Mohr[10], A. Montanari[2], T. Mori[24],
K. Nagai[8], I. Nakamura[24], H.A. Neal[12,f], R. Nisius[8], S.W. O'Neale[1], F.G. Oakham[7],
F. Odorici[2], H.O. Ogren[12], A. Okpara[11], M.J. Oreglia[9], S. Orito[24], G. Pásztor[31],
J.R. Pater[16], G.N. Patrick[20], J. Patt[10], R. Perez-Ochoa[8], S. Petzold[27],
P. Pfeifenschneider[14], J.E. Pilcher[9], J. Pinfold[30], D.E. Plane[8], B. Poli[2], J. Polok[8],
M. Przybycień[8,d], A. Quadt[8], C. Rembser[8], H. Rick[8], S.A. Robins[22], N. Rodning[30],
J.M. Roney[28], S. Rosati[3], K. Roscoe[16], A.M. Rossi[2], Y. Rozen[22], K. Runge[10],
O. Runolfsson[8], D.R. Rust[12], K. Sachs[10], T. Saeki[24], O. Sahr[33], W.M. Sang[25],

1

E.K.G. Sarkisyan[23], C. Sbarra[28], A.D. Schaile[33], O. Schaile[33], P. Scharff-Hansen[8],
J. Schieck[11], S. Schmitt[11], A. Schöning[8], M. Schröder[8], M. Schumacher[3], C. Schwick[8],
W.G. Scott[20], R. Seuster[14,h], T.G. Shears[8], B.C. Shen[4], C.H. Shepherd-Themistocleous[5],
P. Sherwood[15], G.P. Siroli[2], A. Skuja[17], A.M. Smith[8], G.A. Snow[17], R. Sobie[28],
S. Söldner-Rembold[10,e], S. Spagnolo[20], M. Sproston[20], A. Stahl[3], K. Stephens[16], K. Stoll[10],
D. Strom[19], R. Ströhmer[33], B. Surrow[8], S.D. Talbot[1], P. Taras[18], S. Tarem[22], R. Teuscher[9],
M. Thiergen[10], J. Thomas[15], M.A. Thomson[8], E. Torrence[8], S. Towers[6], T. Trefzger[33],
I. Trigger[18], Z. Trócsányi[32,g], E. Tsur[23], M.F. Turner-Watson[1], I. Ueda[24],
R. Van Kooten[12], P. Vannerem[10], M. Verzocchi[8], H. Voss[3], F. Wäckerle[10], D. Waller[6],
C.P. Ward[5], D.R. Ward[5], P.M. Watkins[1], A.T. Watson[1], N.K. Watson[1], P.S. Wells[8],
T. Wengler[8], N. Wermes[3], D. Wetterling[11] J.S. White[6], G.W. Wilson[16], J.A. Wilson[1],
T.R. Wyatt[16], S. Yamashita[24], V. Zacek[18], D. Zer-Zion[8]

[1]School of Physics and Astronomy, University of Birmingham, Birmingham B15 2TT, UK
[2]Dipartimento di Fisica dell' Università di Bologna and INFN, I-40126 Bologna, Italy
[3]Physikalisches Institut, Universität Bonn, D-53115 Bonn, Germany
[4]Department of Physics, University of California, Riverside CA 92521, USA
[5]Cavendish Laboratory, Cambridge CB3 0HE, UK
[6]Ottawa-Carleton Institute for Physics, Department of Physics, Carleton University, Ottawa, Ontario K1S 5B6, Canada
[7]Centre for Research in Particle Physics, Carleton University, Ottawa, Ontario K1S 5B6, Canada
[8]CERN, European Organisation for Particle Physics, CH-1211 Geneva 23, Switzerland
[9]Enrico Fermi Institute and Department of Physics, University of Chicago, Chicago IL 60637, USA
[10]Fakultät für Physik, Albert Ludwigs Universität, D-79104 Freiburg, Germany
[11]Physikalisches Institut, Universität Heidelberg, D-69120 Heidelberg, Germany
[12]Indiana University, Department of Physics, Swain Hall West 117, Bloomington IN 47405, USA
[13]Queen Mary and Westfield College, University of London, London E1 4NS, UK
[14]Technische Hochschule Aachen, III Physikalisches Institut, Sommerfeldstrasse 26-28, D-52056 Aachen, Germany
[15]University College London, London WC1E 6BT, UK
[16]Department of Physics, Schuster Laboratory, The University, Manchester M13 9PL, UK
[17]Department of Physics, University of Maryland, College Park, MD 20742, USA
[18]Laboratoire de Physique Nucléaire, Université de Montréal, Montréal, Quebec H3C 3J7, Canada
[19]University of Oregon, Department of Physics, Eugene OR 97403, USA
[20]CLRC Rutherford Appleton Laboratory, Chilton, Didcot, Oxfordshire OX11 0QX, UK
[22]Department of Physics, Technion-Israel Institute of Technology, Haifa 32000, Israel
[23]Department of Physics and Astronomy, Tel Aviv University, Tel Aviv 69978, Israel
[24]International Centre for Elementary Particle Physics and Department of Physics, University of Tokyo, Tokyo 113-0033, and Kobe University, Kobe 657-8501, Japan
[25]Institute of Physical and Environmental Sciences, Brunel University, Uxbridge,

Middlesex UB8 3PH, UK

[26]Particle Physics Department, Weizmann Institute of Science, Rehovot 76100, Israel

[27]Universität Hamburg/DESY, II Institut für Experimental Physik, Notkestrasse 85, D-22607 Hamburg, Germany

[28]University of Victoria, Department of Physics, P O Box 3055, Victoria BC V8W 3P6, Canada

[29]University of British Columbia, Department of Physics, Vancouver BC V6T 1Z1, Canada

[30]University of Alberta, Department of Physics, Edmonton AB T6G 2J1, Canada

[31]Research Institute for Particle and Nuclear Physics, H-1525 Budapest, P O Box 49, Hungary

[32]Institute of Nuclear Research, H-4001 Debrecen, P O Box 51, Hungary

[33]Ludwigs-Maximilians-Universität München, Sektion Physik, Am Coulombwall 1, D-85748 Garching, Germany

[a] and at TRIUMF, Vancouver, Canada V6T 2A3

[b] and Royal Society University Research Fellow

[c] and Institute of Nuclear Research, Debrecen, Hungary

[d] and University of Mining and Metallurgy, Cracow

[e] and Heisenberg Fellow

[f] now at Yale University, Dept of Physics, New Haven, USA

[g] and Department of Experimental Physics, Lajos Kossuth University, Debrecen, Hungary

[h] and MPI München

[i] now at MPI für Physik, 80805 München.

1   Introduction

By identifying the flavour of the quark from which a jet develops one can experimentally test both electroweak and QCD theories. The power of flavour tagging has been demonstrated in many studies of bottom and charm quark production. Tagging light quark jets is experimentally much more difficult as these jets are not as distinctive as bottom quark or charm quark jets. The main reason is that, unlike the heavy bottom and charm quarks, production of extra secondary up, down and strange quarks is abundant in jet development, making the identification of the hadron containing the primary quark ambiguous. Due to these difficulties, tagging of individual light quarks has been studied and used in only a few analyses, for example in [1–3].

Whereas most of these analyses make assumptions about the details of hadronisation models, a method has been suggested in [4] which reduces the reliance on these assumptions. This method has already been applied to determine the electroweak observables of individual light flavours by OPAL [2] at the e^+e^- collider LEP. In the present analysis, high-energy $\pi^\pm$, $K^\pm$, K_S^0 mesons, protons and Λ baryons are identified in the large Z^0 data sample and used as tagging particles. In addition, high-momentum $e^\pm$, $\mu^\pm$, $D^{*\pm}$ mesons and identified bottom events are used to provide information about the heavy flavour backgrounds in these samples. As suggested in [5] and first confirmed by TASSO [6] and more precisely studied in recent analyses, for example by SLD [7], these high-energy particles carry information about the original quark. In this paper we extend the method used in Reference [2] to determine the probabilities $\eta_q^i(x_p)$ for a quark flavour q to develop into a jet in which the particle with the largest scaled momentum $x_p = 2p_i/\sqrt{s}$ is of type i.

The large number of Z^0 decays collected at LEP and their well-known properties give a unique opportunity for determining the probabilities $\eta_q^i(x_p)$. From these measurements, we infer for the first time the flavour dependent fragmentation functions of light quarks. This allows us to study the hadronisation mechanism at an unprecedented level of detail. From these studies we determine in a direct way the suppression of strange quarks in the QCD sea and obtain insight into baryon production.

Apart from such hadronisation studies, the results may also be applied to different environments. After taking into account QCD scaling violations which can be rather precisely determined, the $\eta_q^i(x_p)$ from the Z^0 allow one to calculate the $\eta_q^i(x_p)$ at other centre-of-mass energies. Possible applications include studies of light flavour production rates at other centre-of-mass energies [4] and the decay properties of the W boson, top quark or, if discovered, the Higgs boson.

Section 2 contains a summary of the method. Section 3 describes the relevant features of the OPAL detector. The event selection and the tagging particle identification are described in Section 4. The determination of the $\eta_q^i(x_p)$ is described in Section 5 and their systematic uncertainties in Section 6. The results are shown and used to determine some properties of hadronisation in Section 7.

2   Method

As detailed in [4,2] the $\eta_q^i(x_p)$ are determined by using tags in event hemispheres[1]. Each event is separated into two hemispheres using the plane perpendicular to the thrust axis containing the interaction point. Each hemisphere is searched for the highest momentum particle, labelled i, subject to a minimum x_p requirement. If there are a number N_q of hemispheres which originate from a quark of type q and a number $N_{q \rightarrow i}(x_p)$ of tagging particles i with a scaled momentum of at least $x_p \equiv x_{\text{cut}}$ in these hemispheres, then the probability to find a tagging particle i with a scaled momentum of at least x_p is:

$$\eta_q^i(x_p) \;=\; \frac{N_{q \rightarrow i}(x_p)}{N_q}.$$

The determination of the true $\eta_q^i(x_p)$ at the "generator level", i.e. corrected for detector efficiencies and misassignment of the several particle types, is the main experimental aim of this paper. The particles considered are those which have a high probability to tag light flavours: $\pi^\pm$, $K^\pm$, K_S^0 mesons, protons, and Λ baryons. Charge conjugation is implied throughout this paper. What can be measured at the "detector level", i.e. before corrections for detector efficiencies etc., are the number of hemispheres tagged by a particle of type i, labelled N_i and called "single-tagged hemispheres", and the number of events containing a tagging particle in both hemispheres, labelled N_{ij} and called "double-tagged events", where i and j are the tagging particle types.

These numbers are related to the probabilities:

$$\frac{N_i}{N_{\text{had}}}(x_p) \;=\; 2 \sum_{q=\text{d,u,s,c,b}} \eta_q^{i,\ \text{exp}}(x_p)\, R_q \tag{1}$$

$$\text{and} \quad \frac{N_{ij}}{N_{\text{had}}}(x_p) \;=\; (2 - \delta_{ij}) \sum_{q=\text{d,u,s,c,b}} \rho_{ij}(x_p)\, \eta_q^{i,\ \text{exp}}(x_p)\, \eta_q^{j,\ \text{exp}}(x_p)\, R_q, \tag{2}$$

where $\delta_{ij} = 1$ if $i = j$ and zero otherwise and N_{had} is the number of hadronic Z^0 decays. The superscript 'exp' denotes that the $\eta_q^i(x_p)$ include possible distortions due to detector effects. The parameters $\rho_{ij}(x_p)$ take into account correlations between the tagging probabilities in opposite hemispheres, due to kinematic or geometrical effects, for example, and will not be equal to unity if such correlations exist. R_q is the hadronic branching fraction of the Z^0 to quarks q:

$$R_q \;=\; \frac{\Gamma_{Z^0 \rightarrow q\bar{q}}}{\Gamma_{\text{had}}}.$$

R_c and R_b are fixed to the LEP average measurements [8]. Given the good agreement of the Standard Model with data [9], in particular the agreement of the measured R_q, we fix R_d/R_{light}, R_u/R_{light} and R_s/R_{light} to their predicted values [10], such that $\sum_q R_q = 1$, where $R_{\text{light}} = R_d + R_u + R_s$.

---

[1]In this analysis, we denote hemispheres as representing quark jets, since we are interested in studying the evolution of primary quarks into different hadron types.

The true $\eta_q^i(x_p)$ are found after correcting for detector efficiencies and misassignment of the tagged samples. The relationship between the true $\eta_q^i(x_p)$ and the observed $\eta_q^{j,\ \mathrm{exp}}(x_p)$ is parametrised by a flow matrix, $\mathcal{E}_j^i$, which is taken from the simulation:

$$\eta_q^{j,\ \mathrm{exp}}(x_p) \;=\; \sum_i \mathcal{E}_j^i \eta_q^i(x_p) \tag{3}$$

$$\mathcal{E}_j^i \;=\; \frac{N_{q\to i\to j}(x_p)^{\mathrm{MC}}}{N_{q\to i}(x_p)^{\mathrm{MC}}}, \tag{4}$$

where the sum over i includes all tagging particle types at the generator level and $N_{q\to i\to j}(x_p)^{\mathrm{MC}}$ is the number of q-flavour Monte Carlo hemispheres tagged by particle i at the generator level but j in the detector. $\mathcal{E}_j^i$ is found to vary slowly with x_p. In addition it is necessary to count events which are untagged at the generator level but still give rise to a tagging particle in the detector and will henceforth be denoted "other background". For example, these events can be tagged by a particle which is not considered in this analysis, such as a stable hyperon (e.g. Σ^-, Ξ^-), or are tagged by a high-momentum particle which has a true momentum slightly below the minimum required x_p due to the finite momentum resolution of the detector.

The system of equations (1) and (2) has 20 equations (5 single and 15 double tags) with 25 unknown $\eta_q^i(x_p)$ for the five quark flavours produced in Z^0 decays. We extend the system of equations in the following two ways:

1. In order to better measure the heavy flavour $\eta_q^i(x_p)$, we include charm and bottom tags by identifying $D^{*\pm}$ mesons, or a vertex displaced from the interaction point. These techniques have been used previously in OPAL papers [11, 12] and are briefly described in Section 4.4. Charged leptons $e^\pm$ and $\mu^\pm$, which mainly tag heavy flavours but are still a source of background in the light flavour charged hadron samples, are also identified and included in the equation system. Note that the vertex tag does not depend on x_p.

2. In order to reduce the number of unknown $\eta_q^i(x_p)$, we invoke hadronisation symmetries such as $\eta_d^{\pi^\pm} = \eta_u^{\pi^\pm}$, which are motivated by the flavour independence of QCD and SU(2) isospin symmetries. They have been extensively discussed in [4] for $x_p > 0.5$. At lower momenta the relations are potentially broken by isospin violating decays, for example $\phi(1020)$ to charged and neutral kaons. Nevertheless, the relations

$$\begin{aligned}
\eta_d^{\pi^\pm} &= \eta_u^{\pi^\pm}, \\
\eta_s^{K^\pm} &= \eta_s^{K^0} \text{ and} \\
\eta_d^{e^\pm} &= \eta_u^{e^\pm}
\end{aligned}$$

are expected to be valid to high precision also after decays. This has been checked using the QCD model JETSET [13] after adjusting the yield and energy dependence of prominent resonances to the measurements at LEP [14]. We find the relations hold to within 2% above $x_p = 0.2$, the range used in this analysis. Here K^0 is made

6

up of both K^0_S and K^0_L, which are assumed to be equal. A relation that is used which is violated by up to 10% at low $x_p \approx 0.2$ due to decays is

$$\eta_d^{\Lambda(\overline{\Lambda})} = \eta_u^{\Lambda(\overline{\Lambda})}.$$

When introducing these hadronisation symmetries into the equation system, we make whatever small corrections for isospin-violating decays are necessary according to the JETSET Monte Carlo. The HERWIG model [15] is not used to check the hadronisation symmetries because it violates SU(2) isospin symmetry for technical reasons [16].

These additions give a total of 54 equations with 41 unknown $\eta_q^i(x_p)$. The equations are solved requiring a minimum $x_p > 0.2$, 0.3, 0.4, 0.5 and 0.6. In this paper, full results are presented for a minimum $x_p > 0.2$ and summarised for the other cut values.

3   The OPAL Detector

The OPAL detector is described in detail in [17]. The relevant features for this analysis are summarised in this Section. OPAL uses a right-handed coordinate system, where the z-axis points along the electron beam, r is the coordinate normal to this axis, and θ and ϕ are the polar and azimuthal angles with respect to z.

The central tracking system, inside a $0.435\,\mathrm{T}$ axial magnetic field, provides a charged track momentum resolution of $\sigma_p/p = 0.02 \oplus 0.0015\,p_t$, where p_t is the momentum component perpendicular to the beam axis in GeV. A silicon microvertex detector [18], close to the interaction point, is surrounded by three drift chambers: a vertex detector, a large volume jet chamber which provides up to 159 space points per track, and z-chambers which give a precise measurement of the polar angle of charged tracks. The large number of samplings in the jet chamber also provides a determination of the specific ionisation energy loss, $\mathrm{d}E/\mathrm{d}x$, with a resolution of $\sigma(\mathrm{d}E/\mathrm{d}x)/(\mathrm{d}E/\mathrm{d}x) \sim 0.032$ [19] in multihadronic events for tracks with $|\cos\theta| < 0.7$ and the maximum number of samplings. At larger $|\cos\theta|$ the resolution is degraded because fewer measured points are available. The $\mathrm{d}E/\mathrm{d}x$ measurements have been calibrated using almost pure control samples of, for example, pions from K^0_S, μ-pair events and photon conversions into electrons, such that the central values are known to $0.10\sigma(\mathrm{d}E/\mathrm{d}x)$ and the resolution to a precision of $10\,\%$ [20]. The electromagnetic calorimeter consists of $11\,704$ lead glass blocks, each subtending a solid angle of $40 \times 40\,\mathrm{mrad}^2$. The muon chambers surround the calorimeter, behind approximately eight absorption lengths of material.

Detector efficiencies and possible detector biases are studied with approximately six million simulated hadronic Z^0 decays generated with the JETSET 7.4 model [13] and passed through a detailed simulation of the OPAL detector [21]. The fragmentation parameters have been tuned to describe event shapes and other distributions as described in [22]. In addition, for fragmentation studies one million fully-simulated hadronic Z^0 decays generated with the HERWIG 5.8 [15] Monte Carlo generator are used.

4 Event Selection and Tagging Methods

The analysis uses approximately 4.1 million multihadronic Z^0 decays collected between 1991 and 1995. The standard OPAL multihadronic selection is applied [23]. To select events which are well contained in the detector, the polar angle of the thrust axis, θ_T, calculated using charged tracks and electromagnetic calorimeter clusters which have no associated track in the jet chamber is required to satisfy $|\cos\theta_T| < 0.8$. To assure good bottom quark tagging quality it was also required that the silicon microvertex detector be functioning well.

In this analysis we select tagging particles with $x_p > 0.2$. The selection of these highly energetic particles enhances the background fraction from $Z^0 \to \tau^+\tau^-$ events, so we require in addition each event to have at least eight well-measured tracks [24]. With these requirements, $2\,820\,220$ events are retained. In this event sample the τ background is reduced to less than $0.03\,\%$, as estimated using fully simulated events generated with the KORALZ Monte Carlo generator [25], and so can be neglected.

Next a high-energy stable particle or a charm or bottom tag is required. The selection of particles was optimised for the highest accuracy of the desired $\eta_q^i(x_p)$, balancing the potential loss in separation power against efficiencies. As discussed in Section 2, we look for the particle ($\pi^\pm$, $K^\pm$, $p(\bar{p})$, K_S^0, $\Lambda(\bar{\Lambda})$, $e^\pm$, $\mu^\pm$ or $D^{*\pm}$,) in each event hemisphere with the highest scaled momentum x_p. To ensure good charged pion, kaon and proton separation, and reliable K_S^0 and Λ reconstruction, we require that the tagging particles have polar angles $|\cos\theta| < 0.9$.

4.1 Stable hadrons

The $\mathrm{d}E/\mathrm{d}x$ measurement of good quality tracks is used to identify charged pions, charged kaons and protons. For each track the $\mathrm{d}E/\mathrm{d}x$ weight w_i is used to separate the particle types. The weight is the χ^2 probability that the track is consistent with a hypothesised particle i. We require:

- for pion candidates: $w_{\pi^\pm} > 0.1$ and $w_{K^\pm} < 0.1$;

- for kaon candidates: $w_{K^\pm} > 0.1$ and $w_{\pi^\pm} < 0.1$;

- for proton candidates: $w_{p(\bar{p})} > 0.1$ and $w_{K^\pm} < 0.1$.

These selection criteria give three disjoint samples.

Averaged over all five quark flavours,

$$\mathcal{P}_j^i(x_p) = \frac{\sum_q \mathcal{E}_j^i \eta_q^i(x_p)}{\sum_q \eta_q^{j,\,\exp}(x_p)}$$

express the probability that a particle identified as type j stems from a true particle type i. The values are given in Table 1 for samples with $x_p > 0.2$. The determination of the flow matrix $\mathcal{E}_j^i$, which is taken from simulation, was discussed in Section 2. As also discussed in Section 2, a few percent of the tagging particles have a true x_p value below the cut imposed on the measured x_p value but are tagged in the detector due to the finite

momentum resolution. The Monte Carlo also predicts that there is a 1% contamination from charged hyperons, mostly Σ^-, in the proton sample. These sources of background are included in "other background" given in Table 1. The cuts, including the event and thrust axis cut, lead to the efficiencies shown in the bottom row of Table 1, which are defined as the number of hemispheres which are correctly tagged at the detector level divided by the number of hemispheres which are tagged at the generator level.

4.2 Electron and muon identification

Electrons are identified using a number of discriminating variables, principally the $\mathrm{d}E/\mathrm{d}x$ and the energy loss in the electromagnetic calorimeter [12]. Muons are selected by matching tracks in the central detector with hits in the muon chambers [12]. As can be seen from Table 1, the efficiencies to correctly tag an electron or a muon are about 20% and 70% in this hadronic jet environment, respectively, with purities of around 60%.

4.3 K_S^0 and Λ identification

The procedures to identify the weakly decaying K_S^0 and Λ are described in [26] and [27], respectively. The decays $K_S^0 \to \pi^+\pi^-$ and $\Lambda \to p\pi^-$ are reconstructed by combining two oppositely-charged tracks which have a crossing point in the plane orthogonal to the beam axis. If a secondary vertex is found, the invariant masses $m_{\pi^+\pi^-}$ and $m_{p\pi^-}$ of the $\pi^+\pi^-$ and $p\pi^-$ mass assignments are calculated. K_S^0 candidates are required to have invariant masses in the ranges $430\,\mathrm{MeV} < m_{\pi^+\pi^-} < 570$ MeV and $m_{p\pi^-} > 1.13\,\mathrm{GeV}$, to reduce the contamination from $\Lambda \to p\pi^-$ decays. Similarly, all candidates which have 1.10 GeV $< m_{p\pi^-} < 1.13\,\mathrm{GeV}$ are accepted as Λ candidates. The K_S^0 selection in [26] is extended in the present analysis to $|\cos\theta| < 0.9$ from 0.7, resulting in a slightly worse overall mass resolution, but the acceptance is increased and is the same as the other particle tags used, thus reducing geometric hemisphere correlations. The combinatoric backgrounds are estimated from the Monte Carlo and cross-checked by determining the backgrounds from candidates with invariant masses in sidebands around the signal.

4.4 Charm quark and bottom quark tags

The sample enriched in charm quark events is found by selecting hemispheres with a high-energy $\mathrm{D}^{*\pm}$ [11]. The decay modes and the cuts used on the $x_p^{\mathrm{D}^*}$ values, which are calculated from the measured decay products of the $\mathrm{D}^{*\pm}$ candidate, are

$$
\begin{aligned}
&\mathrm{D}^{*+} \to \mathrm{D}^0\pi^+ \\
&\qquad\hookrightarrow \mathrm{K}^-\pi^+ && x_p^{\mathrm{D}^*} > 0.4 \\
&\qquad\hookrightarrow \mathrm{K}^-e^+\nu_e && x_p^{\mathrm{D}^*} > 0.4 \\
&\qquad\hookrightarrow \mathrm{K}^-\mu^+\nu_\mu && x_p^{\mathrm{D}^*} > 0.4 \\
&\qquad\hookrightarrow \mathrm{K}^-\pi^+ && x_p^{\mathrm{D}^*} > 0.4 \\
&\qquad\hookrightarrow \mathrm{K}^-\pi^+\pi^-\pi^+ && x_p^{\mathrm{D}^*} > 0.5
\end{aligned}
$$

In the simulation the $\mathrm{D}^{*\pm}$ tagging efficiency is about 1% for a charm quark purity of about 58%.

The bottom quark tag uses a number of discriminating variables calculated from a reconstructed secondary vertex [12]. From the number of double and single-tagged events the hemisphere tagging efficiency is found to be about 19% for a bottom jet purity of about 96%. These efficiencies and purities are used only for the cross-check outlined in Section 6.2. The hemispheres tagged as bottom are counted even if they are already present in the high x_p tagged samples.

5   Determination of $\eta_q^i(x_p)$

The numbers N_i and N_{ij} of measured single- and double-tagged events are given in Table 2 for $x_p > 0.2$. They are used as input to the equation system which is solved for the η_q^i by using a χ^2 fit. The χ^2 function is defined as:

$$\chi^2 = \sum_i \Big[\frac{\tilde{N}_i - 2N_{\text{had}} \sum_q R_q \, \tilde{\eta}_q^{i,\ \text{exp}}(x_p)}{\sqrt{\tilde{N}_i}} \Big]^2 \tag{5}$$

$$+ \sum_{i,j} \Big[\frac{N_{ij} - (2 - \delta_{ij})N_{\text{had}}\rho_{ij}(x_p) \sum_q R_q \, \eta_q^{i,\ \text{exp}}(x_p) \, \eta_q^{j,\ \text{exp}}(x_p)}{\sqrt{N_{ij}}} \Big]^2 \tag{6}$$

where

$$\tilde{N}_i = N_i - \sum_j (1 + \delta_{ij})N_{ij} \quad \text{and}$$

$$\tilde{\eta}_q^{i,\ \text{exp}}(x_p) = \eta_q^{i,\ \text{exp}}(x_p) - \sum_j \rho_{ij}(x_p) \, \eta_q^{i,\ \text{exp}}(x_p) \, \eta_q^{j,\ \text{exp}}(x_p)$$

are used to correct for double-counting of hemispheres in the single- and double-tagged samples. These two corrections are necessary to remove double-tagged events from the sample of single-tagged hemispheres.

In addition, the hadronisation symmetries given in Section 2 are used after being corrected for detector effects and making small corrections for isospin-violating decays according to the JETSET Monte Carlo. Furthermore, certain very small, and therefore unmeasurable, η_q^i are fixed to their JETSET values at the generator level, namely: $\eta_{\text{d,u,s}}^{\mu^\pm}$, $\eta_{\text{d,u,s}}^{\text{D}^{*\pm}}$ and $\eta_{\text{d,u,s}}^{\text{b-vtx}}$. The ρ_{ij} parameters, parametrising possible kinematic and geometrical correlations, are taken from the simulation. Geometrical correlations lead in general to a positive correlation $\rho_{ij} \geq 1$. Motivated by simulation studies, the correlation is assumed to be the same for all tagging particle types except for the $\text{D}^{*\pm}$ and the bottom tag. Typical values are $\rho_{ij} = 1.020 \pm 0.002$ at $x_p > 0.2$ and $\rho_{ij} = 1.13 \pm 0.03$ at $x_p > 0.5$, where the errors are from Monte Carlo statistics, and i and j run over all tagging particle types except for $\text{D}^{*\pm}$ and the bottom vertex tag. For the $\text{D}^{*\pm}$ and bottom vertex tags, the correlations are determined individually for each measured double-tagged sample. For example, $\rho_{\pi^\pm \text{D}^{*\pm}} = 1.048 \pm 0.021$ and $\rho_{\pi^\pm \text{b-vtx}} = 1.018 \pm 0.006$ for $x_p^\pi > 0.2$, where the errors are again from Monte Carlo statistics. The extracted $\eta_q^{i,\ \text{exp}}(x_p)$ are corrected for the detector effects using the flow matrix $\mathcal{E}_j^i$ in equation 3.

The results after corrections for detector efficiency and particle misassignment are listed in Table 3 for $x_p > 0.2$. The table also includes the statistical and systematic

uncertainties and a comparison with the JETSET and HERWIG models. We give details of the results only for the tagging particle types which mainly tag light flavours, namely $\pi^{\pm}$, $K^{\pm}$, K_S^0, proton and Λ. The statistical correlations between the parameters are given in Table 4.

The corrected results also for x_p cuts other than $x_p > 0.2$ are summarised in Table 5 with statistical and systematic error combined. Some of the larger $\eta_q^i(x_p)$ are shown in Figures 1- 4. Correlations between the $\eta_q^i(x_p)$ for different particle types and between the values obtained with different x_p cuts are discussed in Section 7.

The solutions were checked to be unique and that the error matrices were positive definite. The χ^2 per degree of freedom of the solutions are typically ≈ 1.2, and are given in Table 5.

6 Systematic Uncertainties

The validity of the method used in this paper is tested using approximately six million hadronic Z^0 decays generated using the JETSET Monte Carlo and including a full simulation of the OPAL detector. The $\eta_q^i(x_p)$ obtained from solving the equation system agree with the Monte Carlo predictions.

6.1 Main uncertainties

The main sources of systematic uncertainty are due to the limited knowledge of the efficiencies and purities of the particle identification. Others are due to the flavour composition of the $D^{*\pm}$ and bottom-tagged samples. The third class of uncertainties is related to opposite-hemisphere correlations in the double-tagged samples. Since these classes of errors are largely uncorrelated, we estimate their individual impact on the $\eta_q^i(x_p)$ and add them quadratically to obtain the overall systematic error. The errors are determined by changing in turn each input parameter according to the estimated individual range of uncertainty, repeating the analysis, and interpreting the shifts as the error contribution. A break down of the individual error contributions for the most important $\eta_q^i(x_p)$ is listed in Table 6 for $x_p > 0.2$. Relative contributions to the systematic error at other minimum values of x_p are similar.

The following systematic uncertainties are considered:

- **Charged particle purity and efficiency:**

  Systematic errors are applied to the charged pion, charged kaon, and proton yields. The uncertainties in these corrections are estimated by varying the widths and mean values of the ionisation energy loss in the simulation according to the uncertainties discussed in Section 3 [20]. These errors are the dominant ones for all $\eta_q^i(x_p)$ of charged hadrons.

  The uncertainties in the electron and muon identification have been discussed in [12]. The error of the electron identification efficiency is due primarily to uncertainties in modelling the dE/dx. The modelling of the muon efficiency has been checked using μ-pair and $e^+e^- \rightarrow e^+e^-\mu^+\mu^-$ events. The effects on the hadron $\eta_q^i(x_p)$ are small and are included in the error due to charged particle efficiency and purity.

11

- **Efficiencies of K^0_S and Λ:**

  The uncertainties of the K^0_S and Λ efficiencies as given for $x_p > 0.2$ in Table 1, for example, are taken into account. Since the relative yields of K^0_S and $K^\pm$ are important for the separation of up and down quark jets, the uncertainty contributes significantly also to the $\eta_q^{K^\pm}$, for example, to $\eta_u^{K^\pm}$ and $\eta_s^{K^\pm}$. The relevant sources of systematic error are described in [26] and [27]. For the K^0_S the systematic errors for the region $0.7 < |\cos\theta| < 0.9$ were taken to be double those in the barrel region, motivated by the factor of two worse mass resolution in the endcap.

- **Charm tag efficiency:**

  The relative uncertainty in the $D^{*\pm}$ reconstruction efficiency was conservatively estimated to be $\pm 10\%$. This source of error has a negligible effect on the results.

- **Hemisphere correlations:**

  Correlations due to kinematic and geometrical effects are accounted for by the ρ_{ij} parameters, which are taken from Monte Carlo simulation. The values of ρ_{ij} are most sensitive to changes in the angular acceptance of the tagging particles and the thrust angle cut. Variations in maximum $|\cos\theta|$ of the tagging particles between 0.7-0.9, and different cuts on the maximum $|\cos\theta_T|$ between 0.7-0.9 show that the changes of the ρ_{ij} are well simulated. A ± 0.01 absolute systematic error, representing the maximal disagreement between data and Monte Carlo, is assigned for the simulation of the ρ_{ij} values.

- **Other background:**

  Contributions to the detector level η_q^i from events which are not tagged at the generator level are taken from the JETSET Monte Carlo events. Such events are mainly due to tags which have a true x_p lower than the minimum x_p cut used but are tagged due to the finite momentum resolution in the detector, spurious tracks, and combinatoric background in the case of the K^0_S and Λ samples. Another source of other background (mainly in the proton sample) is due to stable charged hyperons, mostly Σ^-.

  These backgrounds represent either an absolute contribution to $\eta_q^{i;\,\exp}(x_p)$ or a constant background fraction which scales with the $\eta_q^i(x_p)$. The systematic errors on the estimations of these backgrounds are taken as the differences in the $\eta_q^i(x_p)$ if the analysis is repeated under the two assumptions, namely treating the other background events as a fraction of the detector level $\eta_q^{i;\,\exp}(x_p)$ or as an absolute contribution. This procedure takes into account uncertainties in the JETSET modelling of both the magnitude and the x_p dependence of the background sources.

- **Charm tag background:**

  The flavour composition of the $D^{*\pm}$ sample has been discussed in [11]. The fraction of bottom quark jets in the $D^{*\pm}$ sample can be directly determined. The contribution from gluon splitting $g \to c\bar{c}$ is negligible. The flavour composition of the combinatorial background is taken from Monte Carlo. We varied the contributions

individually by $\pm 50\%$. The corresponding uncertainties have been included in the systematic errors.

- **Fixed quantities:**

  The quantities which were fixed in the fit, namely $\eta_{\mathrm{d,u,s}}^{\mu^\pm}$, $\eta_{\mathrm{d,u,s}}^{\mathrm{D}^{*\pm}}$, and $\eta_{\mathrm{d,u,s}}^{\mathrm{b-vtx}}$, are each in turn varied by $\pm 100\%$ and the corresponding shifts in the η_q^i taken as systematic errors.

- **Hadronisation symmetries:**

  As discussed in Section 2 the hadronisation symmetries used to solve the equation system may be broken by up to 2% at low x_p and 10% for the relation between $\eta_{\mathrm{d}}^\Lambda(x_p)$ and $\eta_{\mathrm{u}}^\Lambda(x_p)$ [4, 13]. The relations are corrected for any breaking which is present in the JETSET Monte Carlo. Assuming a systematic error equal to the maximal allowed breaking, the $\eta_q^i(x_p)$ change only marginally.

- **Z^0 branching ratios:**

  The uncertainties due to the Z^0 branching ratios R_q into quarks have been estimated by varying each fraction within certain limits. In the case of bottom and charm quarks these are given by the rather precise measurements at LEP [8]. Branching fractions into the individual light quarks are less well determined. A direct measurement has only been performed in [2], which we do not consider because it used a variation of the method applied in this paper. However, there are constraints on the electroweak couplings of up and down quarks coming from lepton nucleon scattering and final-state photon radiation from quarks [8] which agree with the Standard Model expectation.

  To take into account uncertainties in the light flavour R_q, we vary $R_i/(R_{\mathrm{d}}+R_{\mathrm{u}}+R_{\mathrm{s}})$ where $i = \mathrm{d, u, s}$ by $\pm 10\%$ from the Standard Model values taking into account their well measured sum $1 - R_{\mathrm{b}} - R_{\mathrm{c}} = 0.606 \pm 0.010$ [8]. The $\eta_q^i(x_p)$ values change by a maximum of 0.5%, and the χ^2 only marginally. Since we assume the Standard Model in this analysis, we do not include this small source of error in the overall systematic errors.

6.2 Cross-check on events with a heavy quark tag

We followed the procedure detailed in [2] in order to make a cross-check of the principal results. Compared to the light flavour tags based on high x_p stable hadrons, the purity of heavy quark tags is much higher. The cross-check makes use of the charm and bottom tag efficiencies and purities from Monte Carlo, mentioned in Section 4.4. By counting the number of light flavour tags in event hemispheres opposite to a heavy flavour tag, one can determine the $\eta_q^{i;\,\mathrm{exp}}(x_p)$ directly without using a large system of equations. This method leads to results which are consistent with those from the main method used in this paper. The agreement between data and the JETSET model is found to be in general quite good. The biggest discrepancy between the data and the prediction of the JETSET model is for $\eta_{\mathrm{c}}^\Lambda(x_p)$, which will be discussed in more detail in Section 7.1.

7   Results and Hadronisation Studies

The $\eta_q^i(x_p)$ values with their statistical and systematic uncertainties are listed in Table 3 for $x_p > 0.2$. The largest η_q^i in light flavours for mesons are shown in Figures 1 and 2 as a function of the cut on x_p. In addition, for baryons, the η_u^p, η_d^p, η_s^Λ and η_c^Λ are shown in Figures 3 and 4.

In most cases only weak correlations exist between the η_q^i for different tagging particles i, though stronger correlations exist between different flavour η_q^i with the same tagging hadron. The statistical correlation coefficients for the most important η_q^i are given in Table 4 for $x_p > 0.2$. These correlations are typical also for the other minimum values of x_p.

In all cases the expected pattern of the leading particles holds: the up and down quarks fragment mostly into pions, whereas the strange quarks fragment mostly into $K^\pm$ and K_S^0, although the fraction of $\pi^\pm$ is sizable also for strange quarks, especially at low x_p. The heavy charm and bottom quarks produce mostly high-energy pions and kaons.

7.1   Comparison to JETSET and HERWIG

We compare the dominant fragmentation functions for the different flavours to the expectations of the HERWIG and JETSET models. The results are shown in Figures 1 and 2 for mesons, and in Figures 3 and 4 for baryons. Note that the data points are shown for different minimum values of the x_p and therefore are correlated. For $x > 0.2$ the JETSET and HERWIG expectations for all determined fragmentation functions are listed together with the data in Table 3.

Hadronisation is quite differently modelled in the two QCD generators. Whereas JETSET uses the Lund string model [28], HERWIG invokes principally the cluster decay mechanism [29]. Both models, JETSET more than HERWIG, contain several parameters which cannot be derived from first principles. For this comparison we use the standard OPAL tuning [22] which is optimised to describe the overall event properties and inclusive particle production. Our measurements of the flavour dependence of the fragmentation function allows us to test the correctness of the model at a new level of detail.

Most of the tagging probabilities are well reproduced by both JETSET and HERWIG. Exceptions are the consistent underestimation in HERWIG of the meson production in bottom events. In addition HERWIG seems to underestimate η_s^π and both HERWIG and JETSET seem to underestimate $\eta_u^{K^\pm}$. The significance of these deviations is, however, only at the level of two standard deviations. The distributions for kaons have a similar shape for the various quark species. The distributions for pions are significantly steeper than those for kaons, which can at least partly be explained by the larger fraction of pions from resonance decays that will be found at lower x_p values. Particularly η_s^π, which can only be due to either decays or if both an up and a down quark are produced from the hadronisation sea, is steeper than η_s^K and η_d^π.

Whereas proton production is reasonably described by JETSET, the HERWIG prediction deviates significantly from the data. The flavour integrated rate [30] is overestimated at high x_p in this model. As can be seen from Table 3, especially the fractions of protons in up and down quark events are higher. In fact the excess in the

HERWIG prediction is almost exclusively due to these quarks, which are in HERWIG for $x_p > 0.2$ about twice as high as in the data. The data also show that the yield of protons from up quarks is higher than that from down quarks. This will be discussed in more detail in Section 7.3.

HERWIG also significantly overestimates Λ production for all light quark species, as can be seen in Figure 4. The overestimation for $\eta_c^\Lambda(x > 0.2)$ is less pronounced; however, the shape of the fragmentation function is softer than in the data. In the case of Λ baryons in strange and charm events, the JETSET expectation differs from the data as seen in Figure 4. The s $\rightarrow \Lambda$ yield in the data is only about half of that expected although the shape is consistent. For c $\rightarrow \Lambda$ the yield is underestimated by a factor of $2-3$ and the x-dependence tends to be steeper. To study whether the discrepancy in the rate may be due to the analysis procedure, we compare Λ production directly in data and in the JETSET simulation including detector effects. To enrich charm and strange events, respectively, we search for Λ in hemispheres opposite to a tagged D^{*-} or K^+, and $\overline{\Lambda}$ production in hemispheres opposite to a tagged D^{*+} or K^-. The resulting $p\pi^-$ mass spectra are shown in Figure 5. The underestimation of the Λ production in charm events in the simulation is clearly visible, as is the overestimation at high x_p of Λ production in strange events.

In addition to studying absolute rates of individual particle species for a specific flavour, as the next step we compare relative yields for the same flavour or the same particle type. These relations may reveal symmetries in the hadronisation mechanism.

7.2   Strange quark fraction in QCD vacuum

In a next step we compare the yield of $K^\pm$ in up and strange quark events and K_S^0 in down and strange events. Within JETSET the ratio of the production yields of the primary hadrons is a direct measure of $\gamma_s = \mathcal{P}(s)/\mathcal{P}(u, d)$, i.e. the relative quark production probabilities in the hadronisation sea. We present the results in Figure 6 and Table 7. The full lines show the expected ratio in JETSET for a γ_s value indicated by the dotted lines. The difference of up to 10% between the expected ratio and γ_s is due to decays, particularly of the $L = 1$ meson supermultiplet. The comparisons show that $\eta_u^{K^\pm}/\eta_s^{K^\pm}$ (Figure 6a) and $\eta_d^{K^0}/\eta_s^{K^0}$ (Figure 6b) are good estimators of γ_s.

No significant dependence on x_p is observed for either the $K^\pm$ or K_S^0 measurements, which is consistent with expectations. A combined $K^\pm$ and K_S^0 analysis is made by invoking SU(2) isospin symmetry which implies that $\eta_u^{K^\pm} = \eta_d^{K^0}$. After taking into account correlations and correcting for isospin-violating decays at $x_p > 0.2$, we obtain

$$\gamma_s = 0.422 \pm 0.049(\text{stat.}) \pm 0.059(\text{syst.})$$

The systematic uncertainty includes an error of 0.042 to take into account variations of the correction factors due to the uncertain amounts of resonance production, found by varying the contributions of the $L = 1$ meson supermultiplet by $\pm 50\%$.

This value of γ_s is consistent with, although somewhat larger than, previous measurements [31] which are, however, in most cases rather indirect. Comparing the data in more detail with the JETSET prediction in Table 3, one observes that the $\eta_s^{K^\pm}$ and $\eta_s^{K_S^0}$ are in good agreement. However, in the data more $K^\pm$ are found in up quark events and more K_S^0 in down quark events than predicted by JETSET.

In the case of HERWIG the ratios of the flavour dependent K_S^0 and $K^\pm$ production have no simple interpretation in terms of a single parameter. The ratios are fairly similar to those of JETSET and thus agree with the data.

7.3 Baryon hadronisation

The mechanism of how three quarks coalesce in the jet development to form a baryon is still a puzzle of hadronisation. Our measurement of the flavour dependence of the proton and Λ yields provides additional new input.

The ratio η_d^p/η_u^p is shown[2] in Figure 7a and listed in Table 8. Within the LUND string model ideally the ratio η_d^p/η_u^p at high x_p would be a direct measure of the size of the suppression of diquarks [32] with spin 1 relative to spin 0, since Fermi statistics requires a (uu) diquark to have angular momentum $L = 1$. However, decays from heavier baryons such as Λ or Δ resonances tend to change the ratio. Although our result agrees with the production of diquarks as suggested in [32] and already supported by studies of baryon number compensation in jets [33], the uncertainties are so large that the data are also consistent with models that form baryons from quarks that are statistically produced in rapidity. HERWIG, which incorporates a democratic production of diquarks, predicts the production of protons from u and d jets to be more equal than JETSET. The data tend to be smaller than the HERWIG expectation.

We also observe the suppression of strangeness in baryon production by measuring the ratio of Λ baryon production in down and strange quark events. Note that in solving the equation system (6) we have assumed that $\eta_d^\Lambda \sim \eta_u^\Lambda$. After the production of the primary down or strange quark, Λ baryons are formed by picking up a pair of (us) or (ud) quarks, respectively. Indeed fewer Λ baryons are found in down (and hence up) quark jets than in strange jets. The suppression agrees with the JETSET and HERWIG models. The results are shown in Figure 7b and listed in Table 8.

Finally we compare the production of baryons and mesons in events of the same primary quark type. The ratio of proton to pion production in up quark events and the ratio of Λ to charged kaon production in strange events are given in Table 9 and shown in Figures 8a and 8b, respectively. The JETSET expectations fall above the measured data points. Although these measured ratios are poor estimators of the level of diquark suppression (indicated by the dotted line) within the JETSET model due to large contributions from decays, the suppression of baryons relative to mesons is clearly observed. For both ratios the HERWIG expectation is significantly above the measurement as already mentioned in Section 7.1.

In addition one can form the double ratio, $(\eta_s^\Lambda/\eta_s^K)/(\eta_u^p/\eta_u^\pi)$ which within the JETSET model should measure the same quantity $\mathcal{P}(ud)/\mathcal{P}(u)$, modified only by decays, where $\mathcal{P}(x)$ indicates the probability to pick out either a quark or diquark x from the QCD vacuum. The data yield for $x_p > 0.2$

$$\frac{\eta_s^\Lambda/\eta_s^K}{\eta_u^p/\eta_u^\pi} \;=\; 1.23 \pm 0.31,$$

---

[2]The results for $x_p > 0.30$ are not very precise due to a lack of separation power between up and down quarks.

consistent with the JETSET expectation of 1.55, but significantly lower than the HERWIG prediction of 2.24. This indicates that the inclusive baryon production is badly modelled and also the relations between different meson or baryon species are unsatisfactorily simulated in HERWIG.

8   Conclusions

In this paper we have reported on a determination of the probabilities $\eta_q^i(x_p)$ of leading particles to originate from individual quark flavours in Z^0 decays. We studied the production of leading $\pi^\pm$, $K^\pm$, K_S^0, proton, and Λ for $x_p > 0.2$ up to 0.5. The measurement has only a minimal reliance on hadronisation models. In general we observe the expected behaviour that the flavour of the primary quark is reflected in the leading particle, i.e. up and down quarks lead mainly to highly energetic pions, while strange quarks lead mainly to kaons.

These measurements allow several aspects of hadronisation to be studied rather directly, in contrast to many previous analyses which rely strongly on a model unfolding of different contributions. In particular we determine from the relative production of leading charged kaons in up and strange quark jets and leading K_S^0 in down and strange quark jets the suppression of strange quarks in the QCD vacuum:

$$\gamma_s \;=\; 0.422 \pm 0.049(\text{stat.}) \pm 0.059(\text{syst.})$$

We also find that leading protons are more frequent in up than in down quark jets. We also observe the suppression of strange diquarks in $(d, u) \rightarrow \Lambda$ events and baryons relative to mesons in events of the same quark flavour.

For most quark flavours and particle types the JETSET model reproduces the measurements well. A possible exception is the production of Λ baryons in charm quark events which appears to have a higher yield and a harder fragmentation function than expected. HERWIG provides in general a good description of mesons in light quark events but has deficiencies in baryon production, in particular the relative yields of different baryon types and the ratios of baryons and mesons in the same flavour jet.

In addition to these hadronisation studies, our measurements of the $\eta_q^i(x_p)$ may also be interesting for future experiments. In providing tagging probabilities for light flavours with hardly any reliance on hadronisation models, the $\eta_q^i(x_p)$ can be applied at other centre-of-mass energies or in the study of heavy particle decays. This allows a determination of the light flavour production yields and properties in a model-independent way also for environments other than the Z^0.

17

References

[1] OPAL Collaboration, R. Akers *et al.,* Z. Phys. **C60** (1993) 397.

[2] OPAL Collaboration, K. Ackerstaff *et al.,* Z. Phys. **C76** (1997) 387.

[3] DELPHI Collaboration, P. Abreu *et al.,* Z. Phys. **C67** (1995) 1;
DELPHI Collaboration, P. Abreu *et al., Measurement of the Strange Quark Forward-backward Asymmetry around the Z^0 Peak,* CERN-EP/99-134, submitted to Eur. Phys. Jour. C.

[4] J. Letts and P. Mättig, Z. Phys. **C73** (1997) 217.

[5] R. P. Feynman and R. D. Field, Nucl. Phys. **B136** (1978) 1.

[6] TASSO Collaboration, R. Brandelik *et al.,* Phys. Lett. **100B** (1981) 357.

[7] SLD Collaboration, K. Abe *et al.,* Phys. Rev. Lett. **78** (1997) 3442.

[8] C. Caso *et al.,* Eur. Phys. J. **C3** (1998) 1.

[9] See, for example, G. Quast, talk given at EPS-HEP99, Tampere, Finland, July 15-21, 1999.

[10] D. Bardin *et al.,* CERN-TH 6443/92;
D. Bardin *et al.,* Phys. Lett. **B255** (1991) 290;
D. Bardin *et al.,* Nucl. Phys. **B351** (1991) 1;
D. Bardin *et al.,* Z. Phys. **C44** (1989) 493.
We use ZFITTER version 5.0 with default parameters, except `BOXD=1`, `CONV=1`, `INTF=0` and `FINR=0`, and with the following input parameters: m_{Z^0}=91.1863 GeV, m_{top}=175 GeV, m_{Higgs}=300 GeV, $\alpha_{\mathrm{em}}(m_{Z^0})$=1/128.896, $\alpha_s(m_{Z^0})$=0.118.

[11] OPAL Collaboration, K. Ackerstaff *et al.,* Eur. Phys. J. **C1** (1998) 439.

[12] OPAL Collaboration, G. Abbiendi *et al.,* Eur. Phys. J. **C8** (1999) 217.

[13] T. Sjöstrand, Comp. Phys. Comm. **39** (1986) 347;
T. Sjöstrand and M. Bengtsson, Comp. Phys. Comm. **43** (1987) 367;
T. Sjöstrand, CERN-TH.6488/92.

[14] For a review see, for example, I. G. Knowles and G. D. Lafferty, J. Phys. **G23** (1997) 731.

[15] G. Marchesini *et al.,* Comp. Phys. Comm. **67** (1992) 465.

[16] T. Sjöstrand, *QCD Generators,* in "Z Physics at LEP", eds. G. Altarelli, R. Kleiss and C. Verzegnassi, CERN/89-08 (1989), Vol. 3, p. 250.

[17] OPAL Collaboration, K. Ahmet *et al.,* Nucl. Instr. and Meth. **A305** (1991) 275.

[18] P. P. Allport *et al.,* Nucl. Instr. and Meth. **A 324** (1993) 34;
P. P. Allport *et al.,* Nucl. Instr. and Meth. **A 346** (1994) 476.

[19] M. Hauschild *et al.,* Nucl. Instr. and Meth. **A379** (1996) 43.

[20] OPAL Collaboration, G. Abbiendi *et al., Bose-Einstein Correlations in $K^{\pm}K^{\pm}$ Pairs from Z^0 Decays into Two Hadronic Jets,* CERN-EP/99-163, submitted to Eur. Phys. Jour. C.

[21] J. Allison *et al.,* Phys. Rev. **A317** (1992) 47.

[22] OPAL Collaboration, G. Alexander *et al.,* Z. Phys. **C69** (1996) 543.

[23] OPAL Collaboration, G. Alexander *et al.,* Z. Phys. **C52** (1991) 175.

[24] OPAL Collaboration, M. Z. Akrawy *et al.,* Phys. Lett. **B253** (1991) 511.

[25] S. Jadach, B. F. L. Ward and Z. Wąs, Comp. Phys. Comm. **79** (1994) 503.

[26] OPAL Collaboration, R. Akers *et al.,* Z. Phys. **C67** (1995) 389.

[27] See Λ finding method #2 in:
OPAL Collaboration, P. D. Acton *et al.,* Phys. Lett. **B291** (1992) 503;
OPAL Collaboration, G. Alexander *et al.,* Z. Phys. **C73** (1997) 569.

[28] B. Andersson, G. Gustafson, G. Ingelman and T. Sjöstrand, Phys. Rep. **97** (1983) 33.

[29] S. Wolfram, in Proc. 15th Rencontre de Moriond (1980), ed. J. Tran Thanh Van.

[30] OPAL Collaboration, R. Akers *et al.,* Z. Phys. **C63** (1994) 181;
DELPHI Collab., P. Abreu *et al.,* Nucl. Phys. **B444** (1995) 3.

[31] For a compilation see I. G. Knowles, T. Sjöstrand (convs.) *et al.,* in "Physics at LEP2", CERN 96-01, Vol. 2, p. 112, eds. G. Altarelli, T. Sjöstrand, and F. Zwirner.

[32] B. Andersson, G. Gustafson and T. Sjöstrand, Nucl. Phys. **B197** (1982) 45.

[33] For a summary of results before LEP see, for example, P. Mättig, Phys. Rep. **177** (1989) 141.

Assigned	True								
	$\pi^{\pm}$	$K^{\pm}$	$p(\overline{p})$	$e^{\pm}$	$\mu^{\pm}$	K^0_S	$\Lambda(\overline{\Lambda})$	$D^{*\pm}$	other
$\pi^{\pm}$	0.790	0.062	0.003	0.013	0.007	0.038	0.005	0.062	0.019
$K^{\pm}$	0.146	0.568	0.148	0.002	0.002	0.017	0.026	0.071	0.020
$p(\overline{p})$	0.040	0.246	0.551	0.002	0.001	0.014	0.081	0.036	0.031
$e^{\pm}$	0.186	0.023	0.002	0.620	0.000	0.024	0.006	0.128	0.011
$\mu^{\pm}$	0.100	0.061	0.002	0.002	0.643	0.017	0.007	0.153	0.015
K^0_S	0.081	0.030	0.007	0.004	0.001	0.691	0.026	0.101	0.060
$\Lambda(\overline{\Lambda})$	0.047	0.024	0.024	0.003	0.001	0.128	0.696	0.032	0.045
$D^{*\pm}$	0.143	0.074	0.019	0.007	0.006	0.016	0.012	0.699	0.024
efficiency	0.487	0.441	0.292	0.228	0.702	0.155	0.135	0.033	

Table 1: Fractional compositions of the identified samples (rows) in terms of the true tagging particle, for $x_p > 0.2$. The dominant component of other tagged events (last column) is tagging particles which pass the minimum x_p requirement in the detector but whose true momenta are lower. The sum of the elements in each row is one. The last row gives the average efficiency to correctly tag a hemisphere, as taken from Monte Carlo simulation. Errors are discussed in the text.

Particle type	Tagged hemispheres	Double-tagged events								
		$\pi^\pm$	$K^\pm$	$p(\bar{p})$	$e^\pm$	$\mu^\pm$	K^0_S	$\Lambda(\bar{\Lambda})$	$D^{*\pm}$	b-vtx
$\pi^\pm$	855043	71601	77576	16287	7127	7689	10425	4717	2483	25074
	850442	72515	71411	16258	7146	6637	9299	4404	2238	23221
$K^\pm$	506538		25717	10120	4135	4475	7248	3193	1578	14376
	474123		22742	9182	3988	4081	6497	3119	1526	13344
$p(\bar{p})$	101415			963	789	887	1375	591	314	2744
	100046			1019	839	815	1219	583	290	2784
$e^\pm$	54370				501	1294	594	235	225	6219
	56235				479	1186	542	253	219	6221
$\mu^\pm$	65029					905	674	278	293	8898
	60767					838	541	274	262	8254
K^0_S	71218						523	454	239	2074
	64290						423	440	194	1826
$\Lambda(\bar{\Lambda})$	31721							107	111	1026
	30676							95	82	973
$D^{*\pm}$	17432								57	805
	16692								76	791
b-vtx	245451									22472
	246766									23047

Table 2: Number of tagged event hemispheres and double-tagged events for $x_p > 0.2$. The upper numbers are for data and the lower for Monte Carlo, normalised to the same numbers of $Z \to q\bar{q}$ events.

$\eta_{\mathrm{d}}^{\cdot}$	$0.3866 \pm 0.0027 \pm 0.0257$	0.3926	0.3558
$\eta_{\mathrm{u}}^{\pi^{\pm}}$	$0.3831 \pm 0.0026 \pm 0.0256$	0.3891	0.3558
$\eta_{\mathrm{s}}^{\pi^{\pm}}$	$0.1701 \pm 0.0062 \pm 0.0139$	0.1884	0.1367
$\eta_{\mathrm{c}}^{\pi^{\pm}}$	$0.1728 \pm 0.0097 \pm 0.0186$	0.1508	0.1480
$\eta_{\mathrm{b}}^{\pi^{\pm}}$	$0.1350 \pm 0.0020 \pm 0.0093$	0.1226	0.1129
$\eta_{\mathrm{d}}^{\mathrm{K}^{\pm}}$	$0.0617 \pm 0.0102 \pm 0.0080$	0.0517	0.0451
$\eta_{\mathrm{u}}^{\mathrm{K}^{\pm}}$	$0.1227 \pm 0.0136 \pm 0.0244$	0.0687	0.0703
$\eta_{\mathrm{s}}^{\mathrm{K}^{\pm}}$	$0.2390 \pm 0.0056 \pm 0.0187$	0.2294	0.2300
$\eta_{\mathrm{c}}^{\mathrm{K}^{\pm}}$	$0.0952 \pm 0.0100 \pm 0.0208$	0.1123	0.1107
$\eta_{\mathrm{b}}^{\mathrm{K}^{\pm}}$	$0.0623 \pm 0.0017 \pm 0.0066$	0.0530	0.0464
$\eta_{\mathrm{d}}^{\mathrm{p}}$	$0.0362 \pm 0.0063 \pm 0.0075$	0.0356	0.0795
$\eta_{\mathrm{u}}^{\mathrm{p}}$	$0.0569 \pm 0.0086 \pm 0.0109$	0.0666	0.0913
$\eta_{\mathrm{s}}^{\mathrm{p}}$	$0.0328 \pm 0.0042 \pm 0.0084$	0.0232	0.0319
$\eta_{\mathrm{c}}^{\mathrm{p}}$	$0.0246 \pm 0.0058 \pm 0.0071$	0.0266	0.0334
$\eta_{\mathrm{b}}^{\mathrm{p}}$	$0.0232 \pm 0.0010 \pm 0.0045$	0.0253	0.0199
$\eta_{\mathrm{d}}^{\mathrm{K}_{\mathrm{S}}^{0}}$	$0.0461 \pm 0.0087 \pm 0.0061$	0.0350	0.0345
$\eta_{\mathrm{u}}^{\mathrm{K}_{\mathrm{S}}^{0}}$	$0.0228 \pm 0.0107 \pm 0.0100$	0.0251	0.0229
$\eta_{\mathrm{s}}^{\mathrm{K}_{\mathrm{S}}^{0}}$	$0.1210 \pm 0.0028 \pm 0.0096$	0.1161	0.1160
$\eta_{\mathrm{c}}^{\mathrm{K}_{\mathrm{S}}^{0}}$	$0.0586 \pm 0.0072 \pm 0.0132$	0.0457	0.0505
$\eta_{\mathrm{b}}^{\mathrm{K}_{\mathrm{S}}^{0}}$	$0.0273 \pm 0.0012 \pm 0.0022$	0.0226	0.0195
$\eta_{\mathrm{d}}^{\Lambda}$	$0.0231 \pm 0.0025 \pm 0.0020$	0.0172	0.0566
$\eta_{\mathrm{u}}^{\Lambda}$	$0.0211 \pm 0.0023 \pm 0.0020$	0.0158	0.0542
$\eta_{\mathrm{s}}^{\Lambda}$	$0.0493 \pm 0.0046 \pm 0.0041$	0.0607	0.1325
$\eta_{\mathrm{c}}^{\Lambda}$	$0.0295 \pm 0.0075 \pm 0.0063$	0.0251	0.0480
$\eta_{\mathrm{b}}^{\Lambda}$	$0.0180 \pm 0.0009 \pm 0.0014$	0.0182	0.0170

Table 3: Results for $x_p > 0.2$ after corrections for detector efficiency and particle misassignment. The first error shown is statistical and the second systematic. The two rightmost columns show the JETSET and HERWIG expectations with the OPAL tunings.

	$\eta_{\mathrm{d}}^{\pi^{\pm}}$	$\eta_{\mathrm{s}}^{\pi^{\pm}}$	$\eta_{\mathrm{d}}^{\mathrm{K}^{\pm}}$	$\eta_{\mathrm{u}}^{\mathrm{K}^{\pm}}$	$\eta_{\mathrm{s}}^{\mathrm{K}^{\pm}}$	$\eta_{\mathrm{d}}^{\mathrm{p}}$	$\eta_{\mathrm{u}}^{\mathrm{p}}$	$\eta_{\mathrm{d}}^{\mathrm{K}_{\mathrm{S}}^{0}}$	$\eta_{\mathrm{s}}^{\Lambda}$	$\eta_{\mathrm{c}}^{\Lambda}$
$\eta_{\mathrm{d}}^{\pi^{\pm}}$	1.000	-0.114	-0.117	-0.050	-0.019	0.023	0.006	-0.058	-0.015	-0.008
$\eta_{\mathrm{s}}^{\pi^{\pm}}$		1.000	-0.013	-0.118	-0.334	0.022	-0.088	0.081	-0.029	0.091
$\eta_{\mathrm{d}}^{\mathrm{K}^{\pm}}$			1.000	-0.813	0.250	-0.648	0.503	-0.077	-0.081	0.067
$\eta_{\mathrm{u}}^{\mathrm{K}^{\pm}}$				1.000	-0.354	0.541	-0.603	-0.009	0.127	-0.099
$\eta_{\mathrm{s}}^{\mathrm{K}^{\pm}}$					1.000	-0.091	0.218	0.168	-0.206	0.117
$\eta_{\mathrm{d}}^{\mathrm{p}}$						1.000	-0.825	0.078	-0.015	0.086
$\eta_{\mathrm{u}}^{\mathrm{p}}$							1.000	-0.086	0.047	-0.013
$\eta_{\mathrm{d}}^{\mathrm{K}_{\mathrm{S}}^{0}}$								1.000	-0.018	0.082
$\eta_{\mathrm{s}}^{\Lambda}$									1.000	-0.653
$\eta_{\mathrm{c}}^{\Lambda}$										1.000

Table 4: Statistical correlations between selected parameters for $x_p > 0.2$.

	$x_p > 0.2$	$x_p > 0.3$	$x_p > 0.4$	$x_p > 0.5$	$x_p > 0.6$
$\eta_{\mathrm{d}}^{\pi^{\pm}}$	0.3866±0.0258	0.1924±0.0130	0.0888±0.0062	0.0400±0.0031	0.0183±0.0030
$\eta_{\mathrm{u}}^{\pi^{\pm}}$	0.3831±0.0257	0.1915±0.0131	0.0889±0.0063	0.0400±0.0032	0.0183±0.0031
$\eta_{\mathrm{s}}^{\pi^{\pm}}$	0.1701±0.0152	0.0745±0.0087	0.0280±0.0056	0.0089±0.0029	0.0018±0.0033
$\eta_{\mathrm{c}}^{\pi^{\pm}}$	0.1728±0.0210	0.0652±0.0113	0.0228±0.0068	0.0079±0.0038	0.0013±0.0056
$\eta_{\mathrm{b}}^{\pi^{\pm}}$	0.1350±0.0095	0.0450±0.0033	0.0156±0.0014	0.0051±0.0006	0.0014±0.0005
$\eta_{\mathrm{d}}^{\mathrm{K}^{\pm}}$	0.0617±0.0129	0.0257±0.0152	0.0071±0.0086	0.0011±0.0047	0.0007±0.0179
$\eta_{\mathrm{u}}^{\mathrm{K}^{\pm}}$	0.1227±0.0280	0.0664±0.0265	0.0376±0.0157	0.0195±0.0080	0.0048±0.0204
$\eta_{\mathrm{s}}^{\mathrm{K}^{\pm}}$	0.2390±0.0195	0.1480±0.0116	0.0807±0.0079	0.0385±0.0045	0.0209±0.0041
$\eta_{\mathrm{c}}^{\mathrm{K}^{\pm}}$	0.0952±0.0231	0.0405±0.0130	0.0150±0.0072	0.0070±0.0039	0.0010±0.0045
$\eta_{\mathrm{b}}^{\mathrm{K}^{\pm}}$	0.0623±0.0069	0.0190±0.0024	0.0045±0.0009	0.0007±0.0004	0.0000±0.0008
$\eta_{\mathrm{d}}^{\mathrm{P}}$	0.0362±0.0098	0.0281±0.0100	0.0056±0.0036	0.0008±0.0023	0.0000±0.0085
$\eta_{\mathrm{u}}^{\mathrm{P}}$	0.0569±0.0139	0.0183±0.0120	0.0167±0.0058	0.0050±0.0036	0.0010±0.0055
$\eta_{\mathrm{s}}^{\mathrm{P}}$	0.0328±0.0094	0.0171±0.0059	0.0051±0.0032	0.0044±0.0021	0.0014±0.0022
$\eta_{\mathrm{c}}^{\mathrm{P}}$	0.0246±0.0092	0.0076±0.0047	0.0047±0.0032	0.0006±0.0014	0.0008±0.0033
$\eta_{\mathrm{b}}^{\mathrm{P}}$	0.0232±0.0046	0.0067±0.0015	0.0016±0.0005	0.0004±0.0002	0.0002±0.0001
$\eta_{\mathrm{d}}^{\mathrm{K}_{\mathrm{S}}^{0}}$	0.0461±0.0106	0.0271±0.0144	0.0193±0.0065	0.0114±0.0034	0.0041±0.0162
$\eta_{\mathrm{u}}^{\mathrm{K}_{\mathrm{S}}^{0}}$	0.0228±0.0146	0.0126±0.0177	0.0027±0.0081	0.0000±0.0034	0.0000±0.0206
$\eta_{\mathrm{s}}^{\mathrm{K}_{\mathrm{S}}^{0}}$	0.1210±0.0100	0.0743±0.0059	0.0402±0.0040	0.0192±0.0022	0.0103±0.0020
$\eta_{\mathrm{c}}^{\mathrm{K}_{\mathrm{S}}^{0}}$	0.0586±0.0151	0.0289±0.0084	0.0099±0.0055	0.0043±0.0041	0.0009±0.0040
$\eta_{\mathrm{b}}^{\mathrm{K}_{\mathrm{S}}^{0}}$	0.0271±0.0025	0.0088±0.0013	0.0020±0.0005	0.0002±0.0003	0.0000±0.0001
$\eta_{\mathrm{d}}^{\Lambda}$	0.0231±0.0032	0.0074±0.0025	0.0016±0.0022	0.0017±0.0017	0.0000±0.0003
$\eta_{\mathrm{u}}^{\Lambda}$	0.0211±0.0031	0.0071±0.0024	0.0016±0.0022	0.0017±0.0017	0.0000±0.0003
$\eta_{\mathrm{s}}^{\Lambda}$	0.0493±0.0062	0.0240±0.0058	0.0137±0.0056	0.0077±0.0044	0.0013±0.0043
$\eta_{\mathrm{c}}^{\Lambda}$	0.0295±0.0098	0.0330±0.0088	0.0162±0.0078	0.0010±0.0036	0.0022±0.0093
$\eta_{\mathrm{b}}^{\Lambda}$	0.0180±0.0016	0.0045±0.0009	0.0004±0.0009	0.0000±0.0001	0.0000±0.0001
χ^2	40.8	40.6	53.4	39.4	39.0

Table 5: Results for various values of the minimum x_p requirement with statistical and systematic errors combined. In the last row, the χ^2 of the solution is given. The number of parameters in the fit is 45, of which 32 are free, nine are fixed to their Monte Carlo values and four by hadronisation symmetries.

Source of Error	$\eta_{\mathrm{d}}^{\pi^\pm}$	$\eta_{\mathrm{s}}^{\pi^\pm}$	$\eta_{\mathrm{u}}^{\mathrm{K}^\pm}$	$\eta_{\mathrm{s}}^{\mathrm{K}^\pm}$	$\eta_{\mathrm{u}}^{\mathrm{p}}$	$\eta_{\mathrm{s}}^{\Lambda}$	$\eta_{\mathrm{c}}^{\Lambda}$	$\gamma_{\mathrm{s}}(\mathrm{K}^\pm)$
Charged purity and eff.	0.0254	0.0114	0.0226	0.0176	0.0106	0.0010	0.0004	0.0615
$\mathrm{K}_{\mathrm{S}}^0$ purity and eff.	0.0002	0.0006	0.0048	0.0043	0.0008	0.0006	0.0004	0.0298
Λ purity and eff.	0.0001	0.0001	0.0005	0.0005	0.0007	0.0029	0.0017	0.0011
Charm tag purity and eff.			0.0001				0.0001	0.0003
Hemisphere correlations	0.0012	0.0049	0.0050	0.0033	0.0024	0.0024	0.0057	0.0293
Other background	0.0002	0.0003	0.0008	0.0002	0.0002	0.0003	0.0001	0.0032
Charm tag background	0.0017	0.0061	0.0033	0.0028	0.0006	0.0011	0.0019	0.0121
Fixed quantities $\rightarrow 0$	0.0002	0.0008	0.0006	0.0003	0.0001	0.0001	0.0003	0.0026
Hadronisation symmetries	0.0033	0.0002	0.0039	0.0016	0.0005	0.0004	0.0005	0.0188
δR_{c}	0.0009	0.0004	0.0006	0.0008	0.0001	0.0001	0.0002	0.0043
δR_{b}	0.0001	0.0001	0.0001	0.0001			0.0001	0.0005
Total Systematic Error	0.0257	0.0139	0.0244	0.0187	0.0109	0.0041	0.0063	0.0779

Table 6: Systematic errors on the measurements of the η_q^i, corrected for detector efficiency and particle misassignment, for $x_p > 0.2$. Also shown in the last column are the systematic error contributions for $\gamma_{\mathrm{s}}(\mathrm{K}^\pm)$. Absence of a number means that the error was less than 5×10^{-5}.

x_{cut}	$\gamma_{\mathrm{s}}(\mathrm{K}^{\pm}) = \eta_{\mathrm{u}}^{\mathrm{K}^{\pm}}/\eta_{\mathrm{s}}^{\mathrm{K}^{\pm}}$	$\gamma_{\mathrm{s}}(\mathrm{K}_{\mathrm{S}}^{0}) = \eta_{\mathrm{d}}^{\mathrm{K}_{\mathrm{S}}^{0}}/\eta_{\mathrm{s}}^{\mathrm{K}_{\mathrm{S}}^{0}}$
$x_p > 0.2$	$0.513\pm0.060\pm0.078$	$0.381\pm0.069\pm0.034$
$x_p > 0.3$	$0.448\pm0.117\pm0.123$	$0.365\pm0.127\pm0.152$
$x_p > 0.4$	$0.466\pm0.140\pm0.144$	$0.480\pm0.141\pm0.087$
$x_p > 0.5$	$0.506\pm0.172\pm0.140$	$0.593\pm0.140\pm0.160$
$x_p > 0.2$	$0.422 \pm 0.049 \pm 0.059$	

Table 7: Results for different values of the minimum x_p cut for strange quark suppression as estimated by $\gamma_{\mathrm{s}}(\mathrm{K}^{\pm}) = \eta_{\mathrm{u}}^{\mathrm{K}^{\pm}}/\eta_{\mathrm{s}}^{\mathrm{K}^{\pm}}$ and $\gamma_{\mathrm{s}}(\mathrm{K}_{\mathrm{S}}^{0}) = \eta_{\mathrm{d}}^{\mathrm{K}_{\mathrm{S}}^{0}}/\eta_{\mathrm{s}}^{\mathrm{K}_{\mathrm{S}}^{0}}$ with statistical and systematic errors calculated taking into account correlations between the numerators and denominators of the ratios. In the last row a combined charged and neutral kaon result is given, corrected for decays.

x_{cut}	$\eta_{\mathrm{d}}^{\mathrm{p}}/\eta_{\mathrm{u}}^{\mathrm{p}}$	$\eta_{\mathrm{d}}^{\Lambda}/\eta_{\mathrm{s}}^{\Lambda}$
$x_p > 0.2$	$0.637\pm0.173\pm0.083$	$0.468\pm0.069\pm0.030$
$x_p > 0.3$	$1.54 \pm1.18 \pm0.558$	$0.307\pm0.112\pm0.046$
$x_p > 0.4$	$0.335\pm0.234\pm0.109$	$0.118\pm0.141\pm0.076$
$x_p > 0.5$	$0.165\pm0.421\pm0.257$	$0.221\pm0.264\pm0.173$

Table 8: Results for different values of the minimum x_p cut for uu diquark and strange diquark suppression as estimated by $\eta_{\mathrm{d}}^{\mathrm{p}}/\eta_{\mathrm{u}}^{\mathrm{p}}$ and $\eta_{\mathrm{d}}^{\Lambda}/\eta_{\mathrm{s}}^{\Lambda}$, respectively, with statistical and systematic errors calculated taking into account correlations between the numerators and denominators of the ratios.

x_{cut}	$\eta_{\mathrm{u}}^{\mathrm{p}}/\eta_{\mathrm{u}}^{\pi}$	$\eta_{\mathrm{s}}^{\Lambda}/\eta_{\mathrm{s}}^{\mathrm{K}}$
$x_p > 0.2$	$0.149\pm0.023\pm0.017$	$0.184\pm0.030\pm0.007$
$x_p > 0.3$	$0.096\pm0.056\pm0.030$	$0.162\pm0.041\pm0.006$
$x_p > 0.4$	$0.188\pm0.052\pm0.016$	$0.170\pm0.071\pm0.014$
$x_p > 0.5$	$0.125\pm0.078\pm0.030$	$0.200\pm0.117\pm0.013$

Table 9: Results for different values of the minimum x_p cut for ud diquark suppression as estimated by $\eta_{\mathrm{u}}^{\mathrm{p}}/\eta_{\mathrm{u}}^{\pi}$ and $\eta_{\mathrm{s}}^{\Lambda}/\eta_{\mathrm{s}}^{\mathrm{K}}$, with statistical and systematic errors calculated taking into account correlations between the numerators and denominators of the ratios.
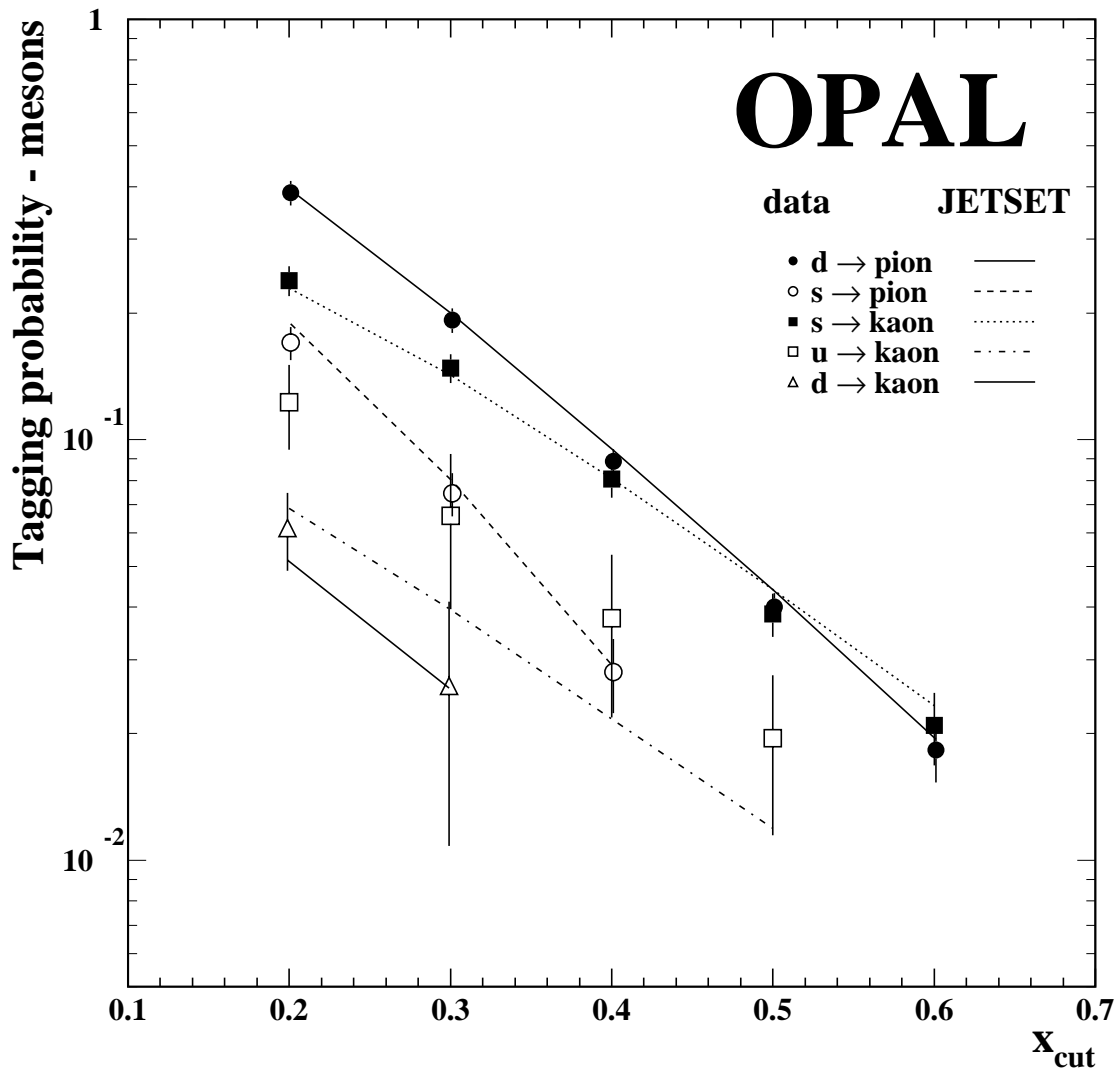
Figure 1: Tagging probabilities as a function of the minimum x_p cut for charged pions and kaons. Data points are correlated for different values of the minimum x_p cut. The errors shown are statistical plus systematic. The lines show the JETSET predictions.
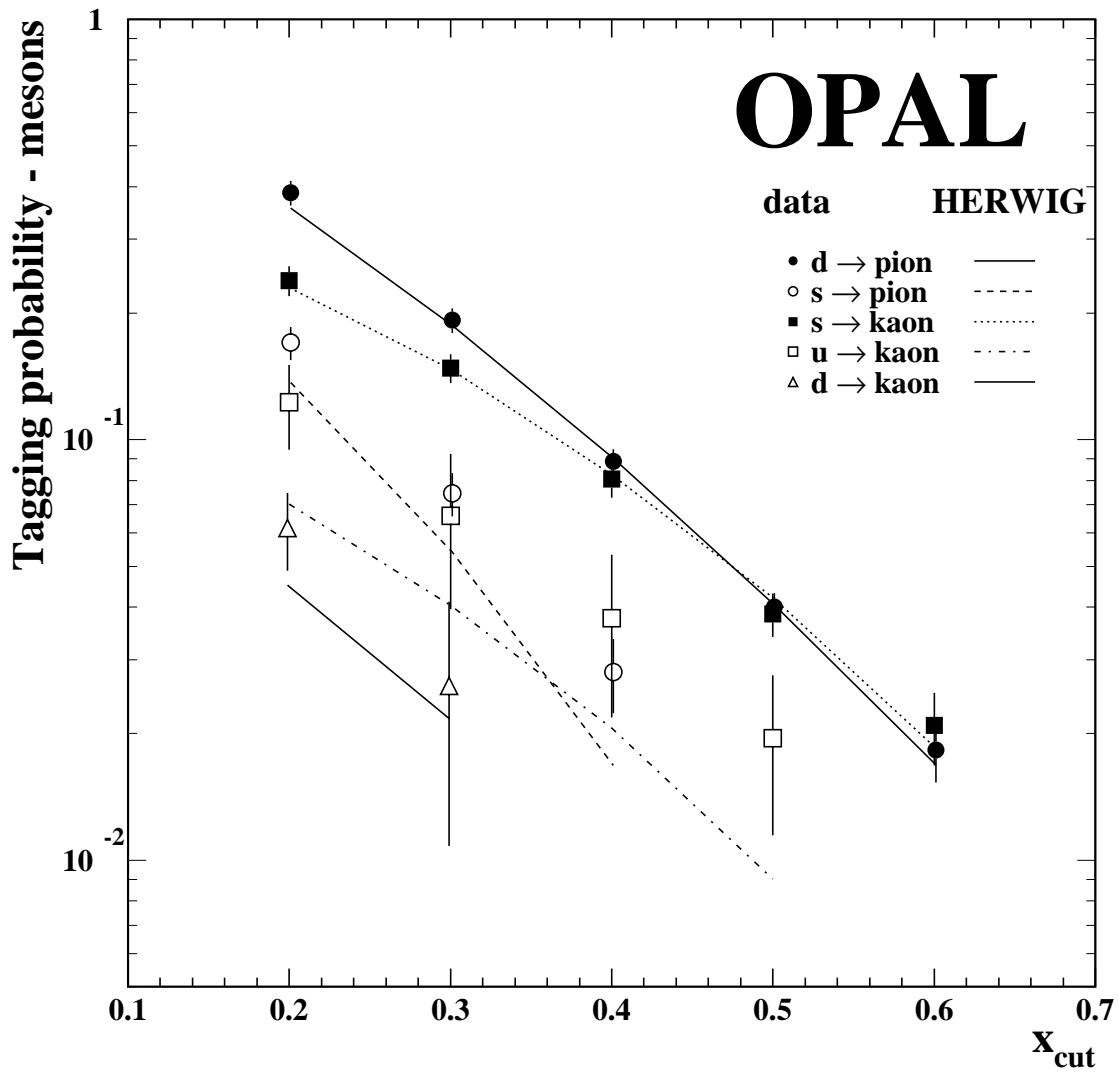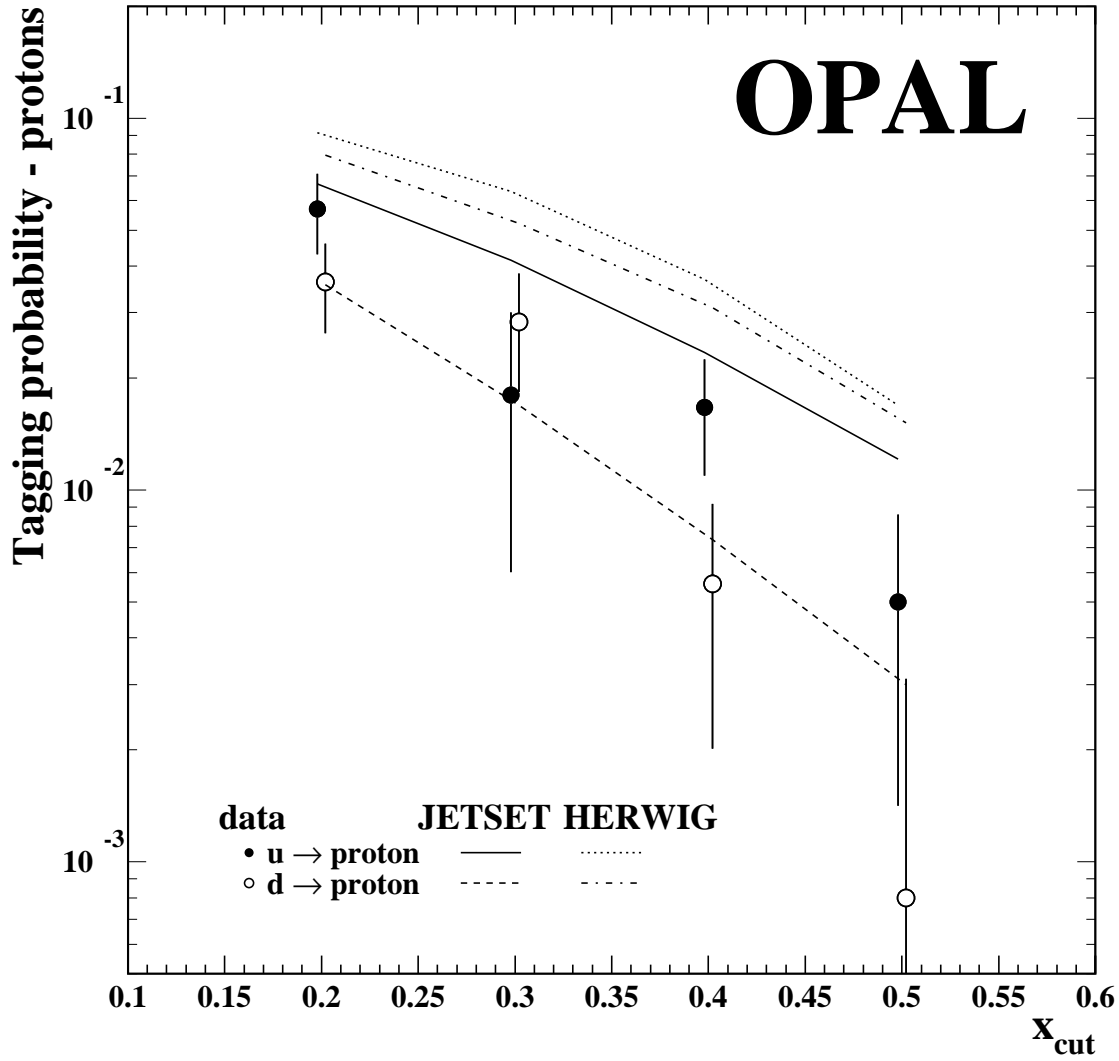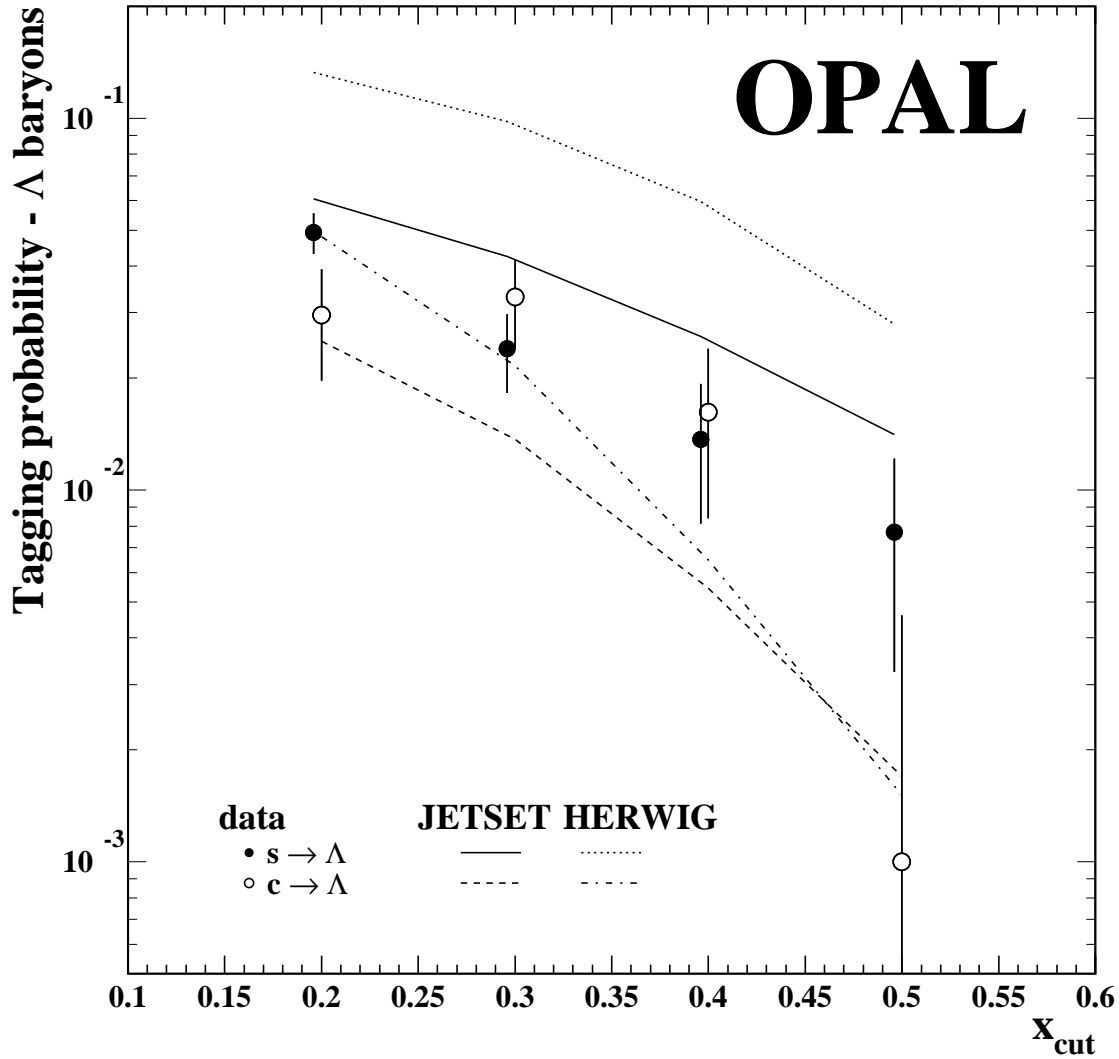
Figure 2: Tagging probabilities as a function of the minimum x_p cut for charged pions and kaons. Data points are correlated for different values of the minimum x_p cut. The errors shown are statistical plus systematic. The lines show the HERWIG predictions.

Figure 3: Tagging probabilities as a function of the minimum x_p cut for protons. Data points are correlated for different values of the minimum x_p cut. The errors shown are statistical plus systematic. The lines show the JETSET and HERWIG predictions.

Figure 4: Tagging probabilities as a function of the minimum x_p cut for Λ baryons. Data points are correlated for different values of the minimum x_p cut. The errors shown are statistical plus systematic. The lines show the JETSET and HERWIG predictions.
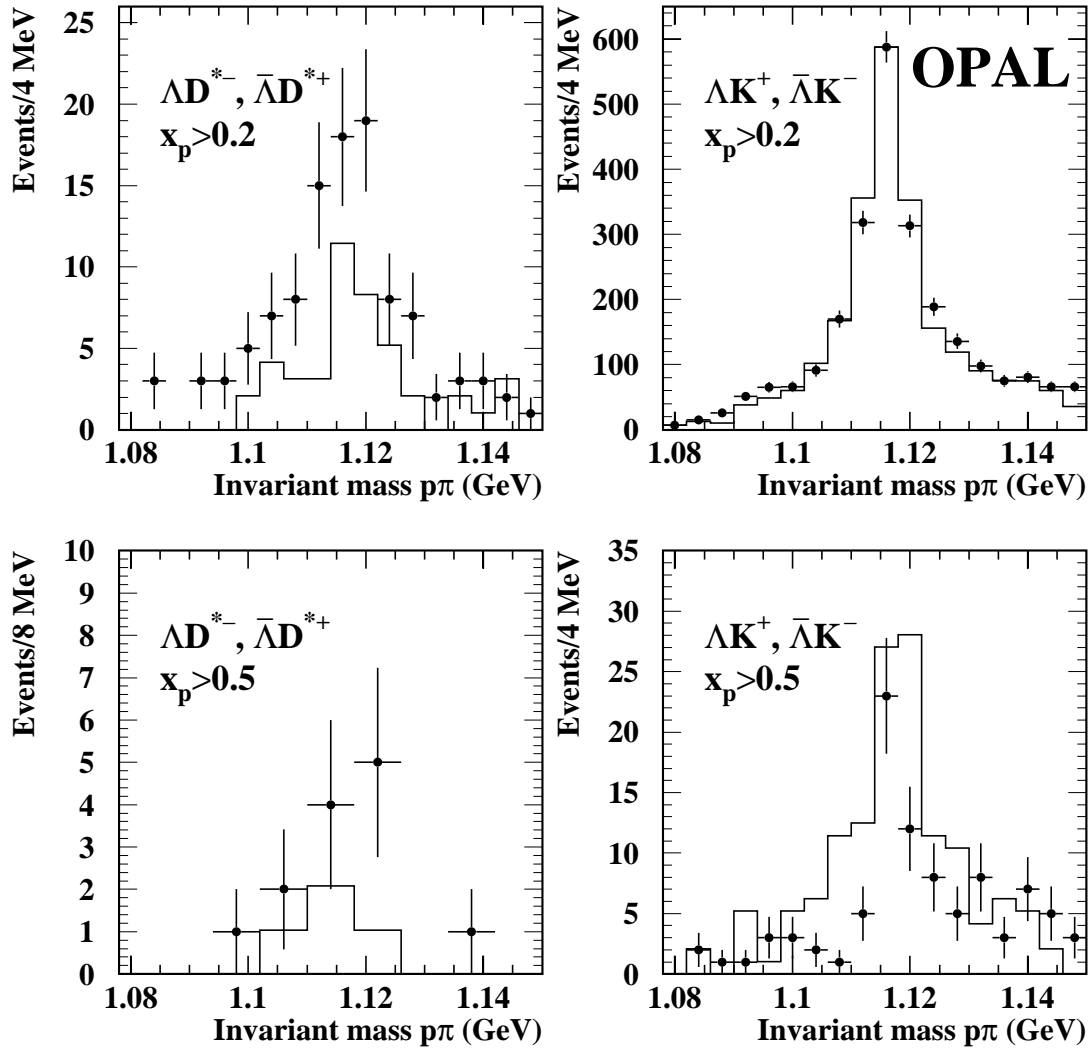
30

Figure 5: Invariant mass distributions for the Λ signals in data (points with error bars) and the JETSET Monte Carlo (histogram). The Monte Carlo is normalised to the same number of events with a D^{*-} (left) or a K^+ (right) in the opposite hemisphere, for two different x_p ranges.
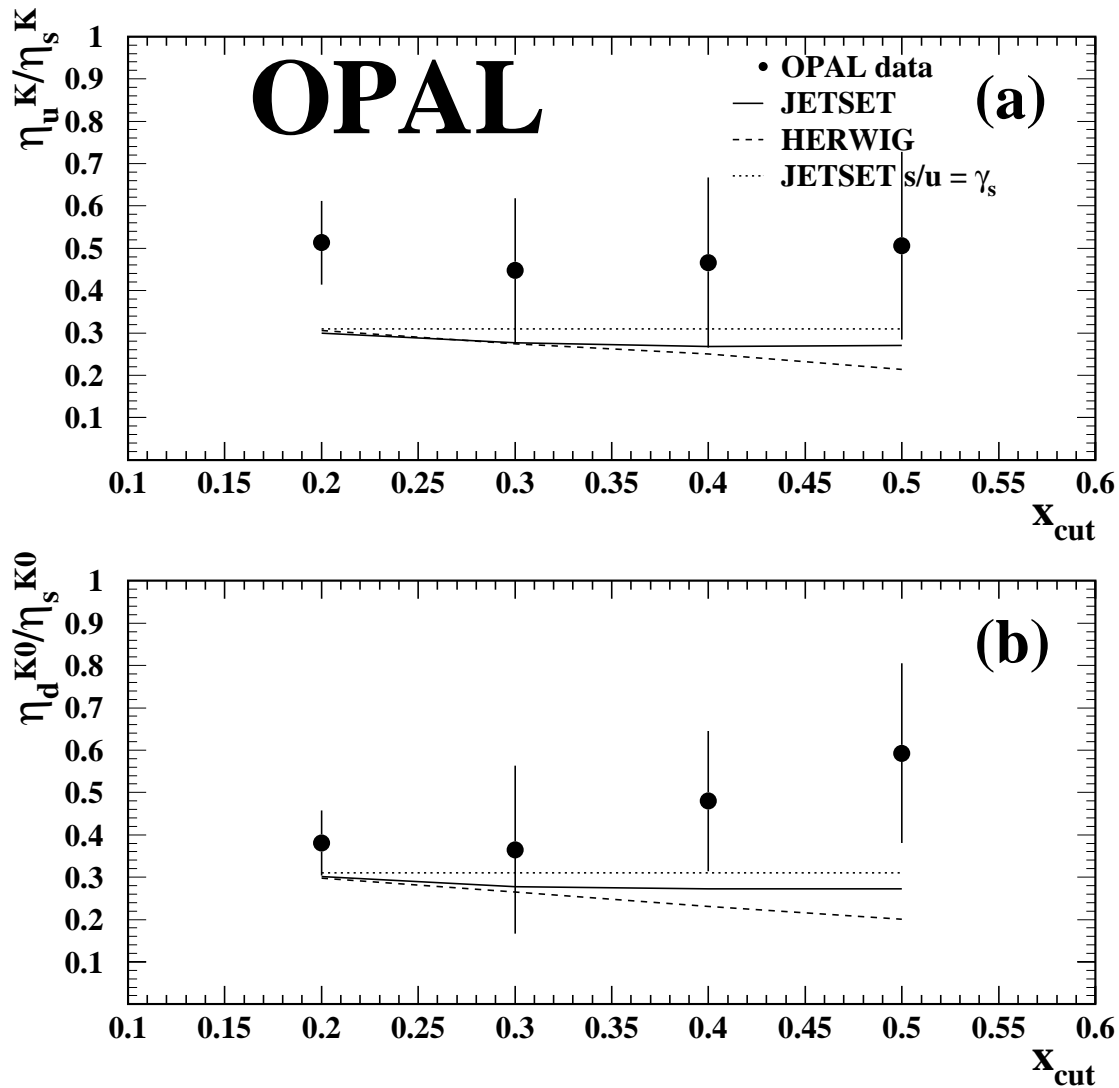
Figure 6: Determination of $\gamma_s = s/u$ using the estimator $\eta_u^{K^\pm}/\eta_s^{K^\pm}$ (a) and $\eta_d^{K_S^0}/\eta_s^{K_S^0}$ in the (b) in the OPAL data (solid points). Data points are correlated for different values of the minimum x_p cut and the errors shown are statistical plus systematic. The solid lines represent the true $\eta_u^{K^\pm}/\eta_s^{K^\pm}$ and $\eta_d^{K_S^0}/\eta_s^{K_S^0}$ in the JETSET Monte Carlo and the dashed lines the HERWIG predictions. The dotted lines represent the input value of $\gamma_s = $ PARJ(2) $= 0.31$ in JETSET.
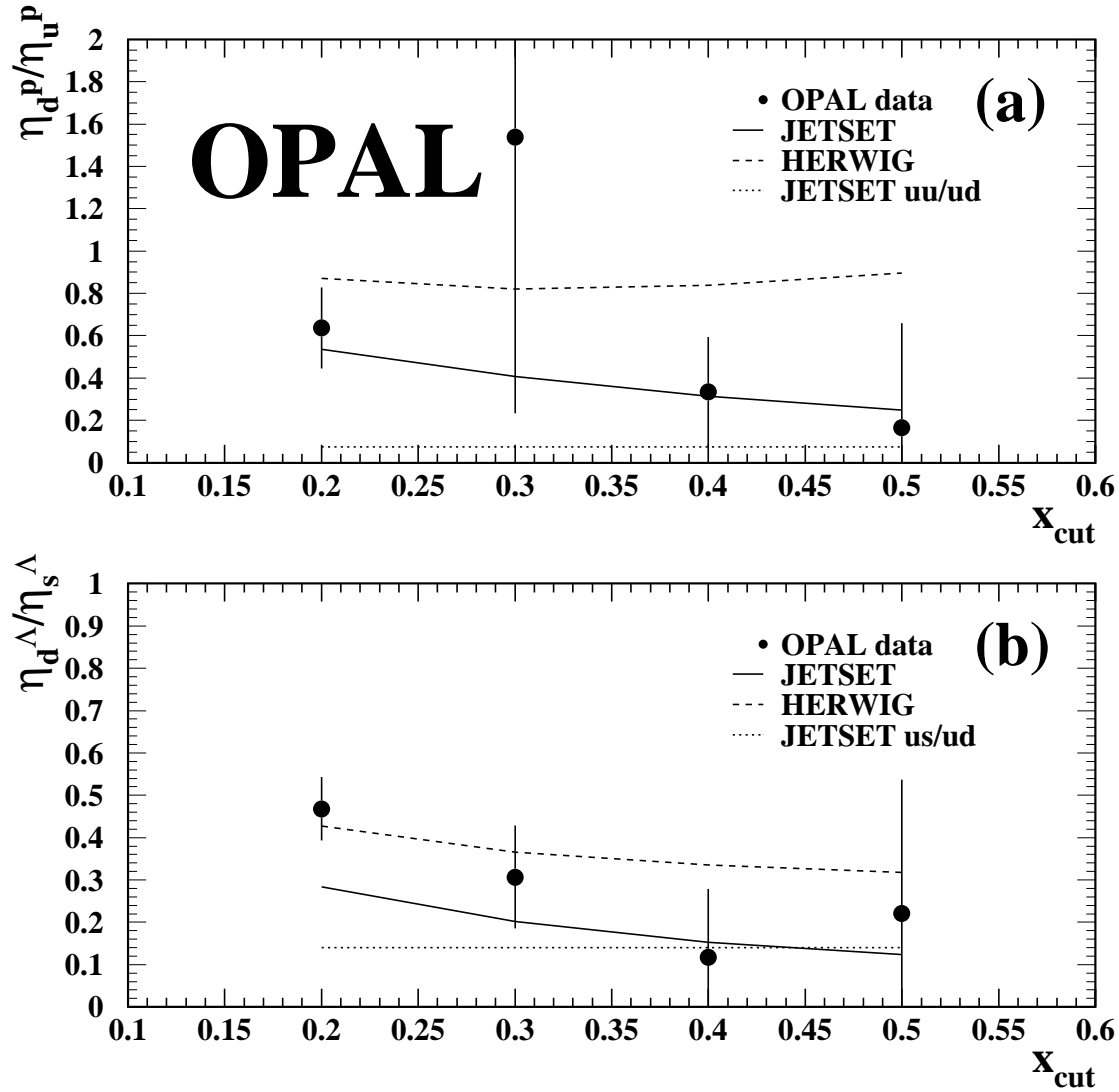
Figure 7: $\eta_{\mathrm{d}}^{\mathrm{p}}/\eta_{\mathrm{u}}^{\mathrm{p}}$ (a) and $\eta_{\mathrm{d}}^{\Lambda}/\eta_{\mathrm{s}}^{\Lambda}$ (b) in the OPAL data (solid points). Data points are correlated for different values of the minimum x_p cut and the errors shown are statistical plus systematic. The solid lines represent the true $\eta_{\mathrm{d}}^{\mathrm{p}}/\eta_{\mathrm{u}}^{\mathrm{p}}$ and $\eta_{\mathrm{d}}^{\Lambda}/\eta_{\mathrm{s}}^{\Lambda}$ in the JETSET Monte Carlo and the dashed lines the HERWIG predictions. The dotted lines represent the input values of uu/ud $= 3 \cdot$ `PARJ(4)` $= 0.075$ (a) and us/ud $= \gamma_{\mathrm{s}} \cdot$ `PARJ(3)` $= 0.1395$ (b) in JETSET.
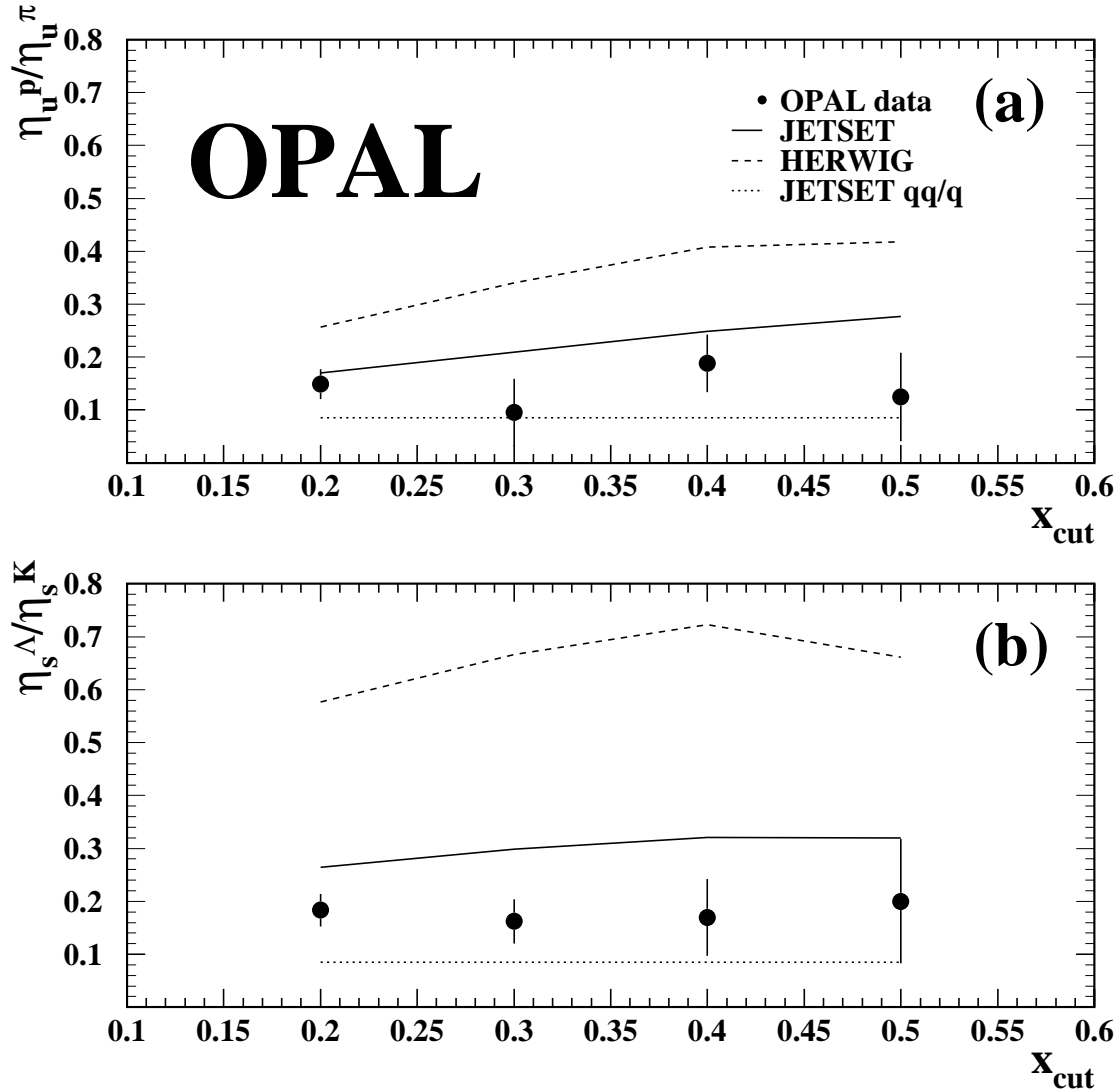
Figure 8: η_u^p/η_u^π (a) and η_s^Λ/η_s^K (b) in the OPAL data (solid points). Data points are correlated for different values of the minimum x_p cut and the errors shown are statistical plus systematic. The solid lines represent the true $\eta_u^p/\eta_u^{\pi^\pm}$ and $\eta_s^\Lambda/\eta_s^{K^\pm}$ in the JETSET Monte Carlo and the dashed lines the HERWIG predictions. The dotted lines show the input values for qq/q = PARJ(1) = 0.085 in JETSET.